Loss of essential outer membrane functions causes drug hypersensitization in *Acinetobacter baumannii* overexpressing multidrug efflux pumps

Efrat Hamami[1], Wenwen Huo[1], Katherine Neal[3], Isabelle Neisewander[1], Edward Geisinger[1,2], Ralph R. Isberg[1,*]

[1]Department of Molecular Biology and Microbiology, Tufts University School of Medicine, 150 Harrison Ave., Boston, MA 02111, USA.

[2]Department of Biology, Northeastern University, Boston, MA, 02115, USA

[3]Department of Biochemistry, Curry College, Milton, MA, USA.

[*]Corresponding Author

Abstract

Elevated expression of Resistance-Nodulation-Cell Division (RND) drug transporters is commonly observed in clinical isolates of *Acinetobacter baumannii*, a nosocomial pathogen associated with multidrug-resistant (MDR) infections. We describe here a CRISPRi platform directed toward identifying essential gene hypomorphs that preferentially change resistance to the fluoroquinolone antibiotic ciprofloxacin in RND pump overproducers. An sgRNA library including single and double nucleotide mutations directed against essential genes of *A. baumannii* was constructed and introduced into multiple strain backgrounds, allowing strain-specific, titratable knockdown efficiencies to be analyzed. Other than NusG depletions, there were few candidates in the absence of drug treatment that showed lowered fitness specifically in strains overexpressing the RND efflux pumps AdeAB, AdeIJK, or AdeFGH. In the presence of ciprofloxacin, the hypomorphs that caused hypersensitivity were predicted to result in outer membrane dysfunction, with the AdeFGH overproducer appearing particularly sensitive to such disruptions. Increased ciprofloxacin susceptibility in two pump hyper-expressers was observed after depletions of a monovalent cation-proton antiporter protein and a nucleoid-associated protein, the latter of which was necessary for pump hyper-activation. On the other hand, depletions of translation-associated proteins as well as components of the proton-pumping ATP synthase resulted in fitness benefits in the presence of the drug for at least two pump-overproducing strains. Therefore, pump overproduction exacerbated stress caused by defective outer membrane integrity, while the efficacy of drug resistance in efflux pump overproducers was enhanced by slowed translation or defects in the proton-pumping ATP synthase.

Importance

Acinetobacter baumannii clinical isolates are increasingly multidrug-resistant, leaving patients with few effective treatment options. Many of these isolates are fluoroquinolone-resistant due to drug target mutations in the two major type II topoisomerases, as well as mutations that activate RND efflux pump expression. This work identifies essential gene products that support the fitness of efflux pump hyperexpressers during treatment with the fluoroquinolone antibiotic ciprofloxacin, most of which are involved in OM biogenesis. These findings suggest new strategies for combination therapy with currently available fluoroquinolones to sensitize and combat high-level resistant strains.

Introduction

Acinetobacter baumannii is a Gram-negative nosocomial pathogen that causes ventilator-associated pneumonia, bacteremia, and urinary tract infections (1-3). The difficulty in combating diseases caused by this often multidrug-resistant (MDR) organism has stimulated the demand for new antimicrobials and improved therapeutic strategies (1, 3). Among the various determinants of resistance to currently available drugs, hyper-expression of drug efflux pumps is commonly associated with MDR across multiple species (4-9). The Resistance-Nodulation-Division (RND) class of efflux pumps provides the most clinically relevant strategy for extruding antibiotics in *A. baumannii*, with the AdeABC, AdeIJK, and AdeFGH efflux pumps frequently associated with MDR (6-9). Therefore, strategies that target isolates overexpressing these pumps or which hypersensitize these strains to currently available antibiotics are of great interest.

For Gram-negative organisms, the primary route to fluoroquinolone resistance (FQR) is via acquisition of mutations in the active sites of the major type II topoisomerases in the cell, DNA gyrase and topoisomerase IV (10). In sequenced *A. baumannii* clinical strains, resistance mutations in both *gyrA* and *parC* are found, encoding the A subunits of gyrase and topo IV, respectively (10). Based on MIC testing and sequencing of isolates, clinical strains also commonly have a third mutation in one of the regulatory genes that activate an RND antibiotic efflux pump. Mutations in these genes, encoded by *adeS*, *adeN*, or *adeL* upregulate the AdeAB(C), AdeIJK, or AdeFGH efflux pumps respectively, and result in high FQR (7, 11-15).

Previous work identified mutations that caused strain-specific vulnerabilities of pump overproduction in nonessential *A. baumannii* genes. These mutations hindered growth of strains overexpressing efflux pumps or synergized with the fluoroquinolone ciprofloxacin (CIP) to hypersensitize the overproducers to the drug (16). Based on that work, lesions in nonessential genes predicted to alter envelope integrity sensitize efflux pump overproducing strains to CIP treatment. Furthermore, the strain with the activating mutation in *adeL* (causing *adeFGH* overexpression) appeared to result in the most significant physiological consequences, with a broader mutation spectrum found to reduce fitness, and a more robust transcriptional shift was apparent relative to the other efflux pump overproducers. These effects may be due to either special features of this pump or extreme overexpression of the *adeFGH* locus relative to the other pump-overexpressing strains (16).

Most effective antimicrobials interfere with proteins essential for growth, making them desirable targets for identifying mutations that preferentially sensitize strains overproducing efflux pumps. To approach this problem, we used CRISPRi to target essential genes with sgRNAs. The library design takes advantage of a previously developed strategy that generates

multiple hypomorphic alleles with varying fitness defects in each essential gene, enabling the discovery of depletions that show strain-specific aggravation of drug sensitivity (17-19). Depletions that cause drug hypersensitivity were found to predominantly target proteins involved in maintaining outer membrane (OM) integrity. Interestingly, interference of translation and the assembly of the proton pumping F_1F_0 ATPase provided the FQR strains with a fitness advantage in the presence of drug. Our work builds on other recent studies using CRISPRi to identify essential *A. baumannii* pathways that alter sensitivities to a large panel of antibiotics (20, 21).

Results

Development of a CRISPRi strategy to uncover hypomorphs with reduced fitness in FQR strains. In our previous study (16), we identified transposon insertion mutations that reduce the fitness of efflux pump overproducers or that specifically hypersensitize these variants to CIP. Except for very rare exceptions (22), insertion mutations could only be analyzed in nonessential genes. This interfered with our ability to identify proteins encoded by the essential gene set that could similarly sensitize pump overproducers. To overcome this limitation, we devised a CRISPRi screening strategy to identify viable depletion variants with drug- or strain-dependent fitness defects (Fig. 1) (17, 18). We applied a pool design similar to that used for eukaryotic cells (17). To identify essential genes, we inspected Tn-seq data from a previously generated dense transposon bank in the ATCC 17978UN strain background (16, 22, 23) for open reading frames (ORFs) having significantly reduced or no insertions (Materials and Methods (24, 25)). After comparison with other published *A. baumannii* Tn-seq studies, a list of 406 essential genes was generated (16, 23, 26, 27).

A single 24-nucleotide (nt) sgRNA was designed for each essential gene by identifying the PAM site on the noncoding strand most proximal to the translational start. For each perfect sgRNA, we devised a set of 23 mismatch sgRNAs that differed from the original guide sequence by 1 or 2 nts at varying locations across the sequence (17). We also created five shuffle sgRNAs comprising the same nts in a disordered fashion to use as negative controls, anticipating that they would have a neutral effect on fitness. Additionally, a collection of approximately 200 shuffle sgRNAs with minimal anticipated genome homology was created, called pool shuffles. The final library consisted of approximately 12,000 sgRNAs with sizes and complexities similar to those of a previously constructed model pool (Fig. 1) (17). To facilitate cloning, the pYDE007 sgRNA delivery vector was converted into a GoldenGate-compatible plasmid to enable efficient construction of the sgRNA library by inserting duplex target oligonucleotides from the pool into the site generated by a Type II restriction enzyme (see Materials and Methods). Control of targeted CRISPRi depletions was provided by an anhydrotetracycline (aTc) inducible dCas9 introduced into the genomes of the WT and FQR pump-overexpressing strains (using a Tn7 strategy originally devised by Peters *et al*. (28) and modified by Bai *et al*. (23); Materials and Methods). The FQR strain panel had the *gyrA parC* (GP) background with either the *adeS*, *adeN*, or *adeL* pump-overproducing mutations (GPS, GPN, and GPL respectively). These strains were then transformed in parallel with the CRISPRi sgRNA plasmid bank, ensuring each pool comprised at least 10^6 transformants.

Mismatched sgRNAs result in a gradient of fitness defects. Pools harbored in all strain backgrounds were cultured in LB for 7-8 generations in the absence or presence of aTc or CIP (Materials and Methods; Fig. 1), with cultures harvested before (timepoint T1) and after bank outgrowth (T2). Plasmid DNA was extracted at both timepoints and the sgRNA region amplified

from the extracted plasmid DNA, barcoded, and sequenced in parallel (Materials and Methods). Reads were processed to determine the abundance of each unique sgRNA at both time points in all conditions. The sgRNA reads showed a normal distribution (Supp. Fig. 1A) that was maintained after introduction into the WT *A. baumannii* strain (Supp. Fig. 1B). A similar distribution was observed from the shuffle sgRNAs after aTc induction (Supp. Fig. 1C), consistent with nontargeting behavior as expected for negative controls. Fitness was calculated after stoichiometric depletion of target genes across replicate cultures as previously described (Materials and Methods (10, 22, 29), with fitness values normalized to a small set of shuffle sgRNAs that had no statistically significant effect on fitness after dCas9 induction. As anticipated, most shuffle guides showed no change in fitness upon dCas9 induction (Fig. 2A), whereas the majority of sgRNAs with perfect target homology showed diminished fitness upon dCas9 induction (73% of perfect guides reducing fitness based on FDR <0.05, fitness < 0.96 after induction compared to control, with fitness at least 10% lower than uninduced cultures; Fig. 2B). Improved fitness was observed by guides harboring mismatched nts closest to the 3' PAM site critical for dCas9 targeting (34% of these guides with mismatched nts most proximal to the PAM site reducing fitness, based on FDR <0.05 and fitness < 0.93 after induction, with fitness lowered by at least 10% from uninduced cultures; Fig. 2C) (17, 18). This pattern can be seen by focusing on sgRNA sets targeting individual genes, such as *gyrA*, which encodes subunit A of DNA gyrase, which showed a broad range of fitness defects depending on the mismatch site (Fig. 2D, E).

The mild effects observed in the remaining 27% of perfect-match sgRNAs could be due to a variety of factors, including the relative distance of the target sequence from the translation start codon. A distinct relationship was difficult to establish, except when comparing fitness

yielded by guides targeting sites 25-40 nts away from the target codon start site versus those recruited to sites only 1-10 nts away (Supp. Fig. 2A-D). As many sgRNAs with high fitness likely resulted from poor target depletion (ex. Supp. Fig. 2E), we determined if continued growth for additional generations (14-16 generations vs. 7-8) could amplify fitness defects. We found that continued growth expanded the number of perfect sgRNAs causing a significant defect (a 35-38% boost in guides with fitness lowered by at least 0.5; Supp. Fig. 3) without a substantial loss of fitness for the shuffle guides (Supp. Fig. 4). These data indicate that the defects observed in hypomorphs can be aggravated by challenging the sgRNA banks for longer periods of time, consistent with the target proteins being subjected to turnover and dilution through bacterial division.

Identification of hypomorphs with significantly altered fitness in the FQR strain backgrounds. To uncover factors that shape fitness of FQR pump hyper-expressing strains, multiple replicates (n=10) of libraries in four strain backgrounds (WT, GPS, GPN, and GPL) were cultured in rich LB broth in the presence of aTc inducer (for dCas9 expression), and fitness scores of hypomorphs were compared between the drug susceptible WT and FQR strains. To identify candidates important for maintaining FQR strain fitness under fluoroquinolone pressure, the libraries were also grown in parallel in the presence of sub-MIC levels of CIP, with concentrations that resulted in 20-30% growth inhibition across the strains. The statistical significance of each depletion (per unique sgRNA) was calculated as a function of the change in fitness between conditions or the difference in fitness between strains, determined by multiple t-test comparisons using an FDR or q value <5% (Materials and Methods) (30). Discoveries showing a significant fitness shift between comparisons were sorted *in silico* to identify sgRNAs yielding fitness scores at least 20% higher (knockdown imparting a fitness benefit or alleviating

an effect) or at least 20% lower (knockdown causing a fitness defect or aggravating an effect). Among these, targets that were represented by 3 or more guides from their sgRNA set were identified as top hits. Targets were identified that fulfilled these criteria during CIP treatment (vs untreated (untx)) and preferentially in the FQR strain (vs WT). Among these, the top candidates were targets identified in more than one FQR strain background.

In the absence of antibiotics, few candidates with three or more guides passed this statistical threshold, further supporting the Tn-seq results indicating that *A. baumannii* is quite tolerant of pump overproduction (Supp. Fig. 5A-C) (16). This was particularly true of the GPS strain, indicating that overproduction of the AdeAB pump is well tolerated by *A. baumannii* (Supp. Fig. 5A, vs. B and C). Loosening the fitness difference criterion (FQR vs WT) from at least 20% to at least 10% identified a total of 28 targets (originally 1) that reduced GPS fitness relative to WT, including proteins involved in secretion across the inner membrane (*secY*, *secA*, *ffh)*, DNA replication, the electron transport chain, and the TCA cycle (Supp. Fig. 5D-E, Supp. Fig. 6A). Doing so also uncovered 9 targets that diminished fitness of all three FQR strains (Supp. Fig. 5D) and 29 in at least two FQR strains (Supp. Fig. 5E).

Outgrowth for additional generations revealed a smaller set of fitness determinants in GPS when compared to WT, only three of which overlap with those identified after 7-8 generations of growth (n=5, Supp. Fig 6B vs. Supp. Fig. 6A). However, it is notable that depletion of factors involved in competing processes resulted in opposing phenotypes after 14-16 generations. For example, depletion of the transcription termination factor Rho improved fitness of the GPS mutant relative to WT, while depletion of the anti-terminator NusG showed stronger fitness defects in GPS (*nusG* and *rho*; Supp. Fig. 6B). Importantly, when considering hypomorphs whose fitness varied by at least 20%, depletion of anti-transcription termination

factor *nusG* was the single target identified as lowering fitness of more than one pump hyper-expresser in the absence of drug pressure. In fact, knockdown of *nusG* showed profound reductions in fitness in all three FQR strains when compared to WT (Supp. Fig. 5A-D). In *E. coli*, NusG-dependent antitermination is tightly linked to the regulation of ribosomal RNA transcription (31, 32).

Depletion of either translation-associated or F_1F_0 ATPase assembly proteins increases CIP tolerance of pump overproducers. Using criteria similar to those used to identify strain-specific fitness differences in the absence of drug, we identified 8 targets with a fitness advantage and 10 candidates with a fitness defect in pump overproducers after exposure to CIP (Supp. Fig. 7). Analysis of pump overproducer and WT depletion derivatives (Figs 3A-F; Supp. Fig. 7A) revealed a clear pattern: the GPL background (Fig. 3C, 3F) generated the most depletions that selectively hypersensitized it to drug relative to WT, with few targets differentiating the GPS and WT backgrounds (compare Fig. 3D to 3E, F). This is consistent with a previous study analyzing mutations in nonessential genes (16). Furthermore, depletions leading to cell envelope integrity dysfunction were the most prominent candidates for CIP synergy, supporting the previous Tn-seq study (16).

Depletion of *lpxC* and *lpxD* genes, encoding LOS biogenesis proteins, uniformly caused fitness defects relative to WT in the presence of drug, even for the robust *adeS* mutant (Fig. 3, Supp. Fig. 7B). With GPN and GPL, the spectrum of depletions that caused fitness defects was expanded to include other loci involved in LOS biosynthesis (*kdtA/waaA*, *kdsD/kpsF*) as well as a large cluster of genes involved in LOS transport to the surface (*lptA-C*, *lptG*) (Fig. 3, Supp. Fig. 7B). These data emphasize that OM integrity maintenance is required for FQR survival in the presence of drug, with factors controlling the composition of LOS being particularly important.

Of note is the fact that depletions of BamD had weaker effects on the GPS pump overproducer than the other two FQR strains, consistent with our observation that there were fewer hypomorphs interfering with composition of the OM that reduced GPS fitness (Fig. 3, Supp. Fig. 7B). Notably, activation of the *adeS*-regulated AdeAB system does not result in overexpression of an OM protein component that would likely be linked to hypersensitizing defects in OM biogenesis (33, 34).

Our most surprising result is that depletion of loci associated with ribosome biogenesis and assembly, as well as translation, strongly increased fitness of at least two FQR strains relative to WT, consistent with slower translational rates increasing fitness of efflux overproducers (Fig. 3 vs. Supp. Fig 7A, Supp. Fig. 7C). Supporting this hypothesis are depletions of *spoT* and *obgE* that similarly increased fitness of the GPL pump overproducer relative to WT (see Supp. Data 4). These are predicted to prevent degradation of ppGpp-associated alarmones, resulting in translational stalling (35, 36). There was also a clear demonstration of increased fitness exhibited by depletions of the F_1F_0 proton-pumping ATPase/synthase in the presence of CIP, tying fitness to the overall proton gradient of the cell (Fig. 3, Supp. Fig. 7C). As the function of the antibiotic efflux pumps is to antiport drugs in exchange for protons, decreased F_1F_0 ATP synthase activity may remove an important competitor for protons or facilitate cytoplasmic pH homeostasis.

Inefficient FQR knockdowns that are hypersensitized to CIP are largely impaired in envelope integrity. We next focused on guides that showed minimal fitness defects in the absence of antibiotic treatment, allowing condition-specific effects to be detected across a large dynamic range (Fig. 4A). This set of sgRNAs, called neutral or enhancer guides, were categorized as those resulting in fitness scores that averaged around 1.00 (neutral) or 1.06

(enhancer) during dCas9 induction in the WT background. They demonstrated no substantial change in fitness between growth in the presence or absence of inducer (fitness score differences within 0.05) (Fig. 4A). Of 284 targets that comprise the neutral and enhancer guide list, excluding shuffles and requiring representation by at least 3 unique sgRNAs, 13 candidates were identified that showed significantly lower fitness in the FQR background compared to WT in the presence of CIP (Fig. 4B, Supp. Data 4). These 13 candidates are predominantly proteins that shape OM integrity, with WaaA and Lpt proteins being top discoveries when restricting guides to those with inefficient knockdown (Fig. 4B).

Of the 13 FQR mutants that were sensitized to CIP, WaaA, LolA, PhaF, IhfB, LptC, LptG, and LpxC were selected for experimental verification. The sgRNAs were chosen based on their strong fitness defects during CIP exposure in GPL and at least one other FQR strain (Fig. 5B-D vs Fig. 5F-H), as well as having minimal effects on WT fitness in the absence or presence of drug (Fig. 5A, Fig. 5E). We observed the strongest fitness deficiencies in the GPL strain background (Fig. 5H), so we created individual sgRNA knockdowns of the top discoveries in GPL and evaluated their growth alongside those in the WT strain background.

CIP stress drives increased dependence of FQR strains on the function of OM and LOS biogenesis proteins. Multiple sgRNAs were tested per target (highlighted in red, blue, or orange spots, with their respective fitness defects during CIP exposure in the pooled screen shown in Fig. 6A). These hypomorphs were cultured individually in the presence and absence of CIP and their growth rates compared to a strain harboring a shuffled non-targeting sgRNA ("NC", NC_159), growing for the same time periods as performed in the screen (Materials and Methods). The doubling times of hypomorphs were then compared to those of the control to detect altered growth rates caused by depletions (Fig. 6B, with the sgRNAs marked the same

way as in Fig. 6A for reference). Depletion of WaaA, LolA, PhaF, LptG, IhfB, LptC, and LpxC all significantly slowed growth of GPL in comparison to WT during CIP exposure (Fig. 6B).

Notably, not all tested sgRNAs yielded the expected phenotype in the GPL background (Supp. Fig. 8A, marked by arrows), but this was linked to poor knockdown, as indicated by qRT-PCR (Supp. Fig. 8B) or poor growth in the absence of the drug. Given the latter reason, additional replicates of LptC and LpxC hypomorphs were tested. Depletions of LpxC and LptC resulted in heightened CIP sensitivity in GPL, with statistical significance only observed for LpxC (Supp. Fig. 9A). Finally, the top 13 candidate hypomorphic guide RNAs were introduced into the GP, GPS, GPN, and GPL strain backgrounds and then cultured individually in the presence or absence of CIP to determine allele specificity. Again, the GPL strain background showed an appreciably heightened sensitivity to CIP upon depletion of all targets of interest, but none significantly altered the growth rate of GPS (Fig. 6C). On the other hand, GPN, which showed more fitness dependencies than GPS (Fig. 5G vs Fig. 5F) exhibited significantly stunted growth compared to GP upon depletion of *waaA*, *ihfB*, and *lpxC* (Fig. 6D). The fact that there were fewer sensitivity loci and much smaller defects than identified for GPL is consistent with our previous analysis of nonessential genes targeted by transposon mutagenesis (16).

To confirm that the defects linked to AdeL were the consequence of efflux pump overexpression, we challenged a derivative of GPL lacking AdeFGH (GPLΔ*adeFGH*) in the presence or absence of CIP (Fig. 6E). In the presence of an intact efflux pump, the doubling time escalated for hypomorphs in the GPL background, with growth rates significantly higher than those observed in the parent GP strain (Fig. 6E). Deletion of the AdeFGH efflux pump reversed this effect, consistent with the vulnerability associated with the *adeL* activation allele being attributed to pump overproduction (Fig. 6E).

Depletion of LOS and lipoproteins impairs membrane integrity, but ZOS and COL amplify CIP selectively in GPL. It is anticipated that depletion of Lpt proteins, as well as other proteins involved in shaping the OM, disrupts membrane integrity. To test for OM dysfunction, hypomorphs were cultured in microtiter plates in the presence of vancomycin (VANC) or sodium dodecyl sulfate (SDS), and their growth was monitored in the absence of any other drug addition (Fig. 7A, B). As expected, depletion of WaaA, LpxC, LolA, LptC, and LptG yielded increased sensitivity to the addition of either vancomycin or sodium dodecyl sulfate, consistent with an impaired membrane barrier in these hypomorphs (Fig. 7A, B).

As depletions of LptC and LptG resulted in strain-specific fitness defects in the presence of CIP, we tested whether we could mimic genetic hypersensitization through the addition of zosurabalpin (ZOS), a drug targeting the $LptB_2FGC$ LPS transporter subcomplex (37). The strains GP, GPL, and GPL lacking AdeFGH were monitored for growth in LB with or without CIP and/or ZOS (Fig. 7C-E). ZOS in combination with CIP dampened the growth of the GPL strain, with the effect stronger than that observed for either drug alone (Fig. 7E). This aggravating effect was not observed in the GP parent strain (Fig. 7C), nor in the GPL strain lacking the AdeFGH efflux pump that is upregulated by the *adeL* mutation (Fig. 7D). An LOS-targeting drug colistin (COL) exhibited even stronger effects (Fig. 7F-H): COL in combination with CIP resulted in a drastic reduction of GPL growth (Fig. 7H). This effect was not detected in GP (Fig. 7F) nor in GPL lacking the AdeFGH pump (Fig. 7G). These results are consistent with the effects of Lpt, WaaA, and LpxC depletions (Fig. 6A, B) and illustrate that identification of mutations that cause aggravating effects also identifies drug targets that aggravate bacterial growth in the presence of a second drug.

Additional essential pathways modulating fitness linked to pump expression during CIP exposure include the IhfB regulator and pH homeostasis. The phenotype of *ihfB* hypomorphs had no direct connection to OM dysfunction, so we considered an alternative model for how they may aggravate fitness during CIP treatment. Given the documented role of IhfB in modulating transcription of numerous genes, including the AcrAB pump activator *robA* in *Salmonella* (38-41), it seemed likely that depletion of *ihfB* altered expression of key resistance determinants in *A. baumannii*. Therefore, transcript levels of *adeG*, encoding the RND protein of the AdeFGH efflux pump, and the *adeL* regulator were determined after IhfB depletion. Depletion of IhfB resulted in a steep decline in *adeG* transcript levels and a corresponding increase in *adeL* expression (Fig. 8A). Therefore, reduction of pump gene expression resulting from IhfB depletion is positively correlated with decreased GPL fitness in the presence of CIP.

In addition to drug sensitizers, we identified hypomorphs that conferred a fitness advantage for efflux pump overexpressers in the presence of CIP. These included strains depleted of inner membrane-associated F_1F_0 ATPase/synthase subunits (*atpI, atpF* in all FQR strains; multiple other *atp* genes in GPL) (Fig. 3D-F). Some studies describe the bidirectionality of the F_1F_0 ATPase/synthase complex, having the ability to both synthesize and hydrolyze ATP using proton motive force (PMF) to drive ATP synthesis or reversibly hydrolyze ATP to pump protons out of the cytosol. ATPase activity, however, was found to be limited and structurally regulated in bacterial species like *A. baumannii*, *E. coli*, and *M. smegmatis*, albeit by different means (42-45). To determine whether the F_1F_0 ATPase/synthase plays a role in maintaining pH homeostasis, intracellular pH (pHi) was measured during AtpF depletion. There was a significant decrease in cytosolic pH as a consequence of depletion (Fig. 8B), linking lowered ATPase activity to the failure to remove protons from the cytoplasm. CIP treatment for 1 hr, however,

eliminated the difference in cytosolic pH between AtpF-depleted and non-depleted cultures (60 µg/mL, mid-exponential phase), indicating that alteration in pH homeostasis may not be a determinant that facilitates drug survival after F_1F_0 ATP synthase depletion (Fig. 8D). On the other hand, in the absence of drug, depletion of PhaF, a CIP sensitizer that modulates the proton gradient as part of a cation/proton antiporter complex (54-56), caused a sharp increase in cytosolic pH (Fig. 8C) that was amplified by CIP exposure (Fig. 8D). Although the exact pHi for WT varied across these experiments, the relative effects of each mutant relative WT were reproducible.

Discussion

Hyperexpression of RND drug efflux pumps often drives MDR, making them excellent targets for antimicrobial therapy. As essential proteins provide particularly attractive targets for the development of new antimicrobials, we knocked down essential genes to identify hypomorphs in strains harboring fluoroquinolone efflux pumps that are specifically sensitized to CIP. This approach showed that depletion of transcripts encoding proteins involved in LOS synthesis and transport, lipoprotein maturation and trafficking to the OM all reduced the fitness of pump overproducers in the presence of antibiotic (CIP) treatment. CIP sensitivity was particularly pronounced in the GPL (AdeFGH pump hyperexpressed) strain, dependent upon the presence of the efflux pump.

BamD, which is necessary to support the fitness of efflux pump overproducers in the presence of CIP, is an outer membrane (OM) component of the Bam complex essential for assembling and properly inserting OM proteins (OMPs) (46). Interestingly, we previously

showed that transposon knockouts of SurA, a non-essential periplasmic chaperone involved in OMP assembly, also decrease the fitness of GPL strains when CIP is present (16, 46-48). Depletions of BamD may interfere with the proper assembly or insertion of the pump OM factor (OMF) or other OMPs that maintain the OM barrier (34). Alternatively, a partially assembled Bam complex may be specifically disruptive to the cell envelope, resulting in the combined defects of periplasmic accumulation of precursors and loss of OMP content, leading to OM dysfunction. Perhaps directly related to this defect, targeting of genes associated with lipoprotein maturation and trafficking (*lnt* and *lolA*) also showed sensitization of efflux pump overproducers. BamD is one of multiple Bam lipoprotein components, consistent with the proposition that depletions of *lnt* or *lolA* could directly phenocopy defects in the Bam complex.

One noteworthy result was that depletions of both LOS synthesis (*waaA*, *kds*, and *lpx* loci) and LOS transport (*lpt* loci) sensitized pump hyperexpressers to CIP. Two earlier reports regarding drug hypersensitivity in *A. baumannii* showed fitness defects that resulted preferentially from defects in LOS transport (21, 49). Decreased levels of Lpt proteins produce a defective cell envelope that results in accumulation of material in the periplasmic space (50, 51). Presumably, the accumulation of LOS precursors inserted into the inner membrane in the absence of Lpt function results in a general sensitivity to most clinically effective antibiotics (21). In contrast to these results, when we focused specifically on strains expressing RND efflux pumps, the spectrum of sensitizing targets was broadened to LOS synthesis (*lpx*), and possibly any factor that disrupts OM biogenesis. In fact, reduced fitness caused by a larger spectrum of defects was predicted by our previous results, which showed that insertion mutations in *lpsB,* which truncates LOS, also diminish the fitness of pump-overexpressing strains during CIP treatment (16, 22).

Targeting proteins that control OM composition and LOS dynamics may diminish the integrity of the OM and facilitate drug entry (Fig. 7A, B), but this alone does not explain why fitness is more severely compromised in the high-level FQR pump hyper-expressers than in the WT or GP strains. One explanation is that LOS directly binds to the RND transporter complex, and the absence of this lipid destabilizes the OM component of the transporter. It is known that LPS can bind OMPs and that OMP-interfacing lipids may mediate protein self-association, contributing to OM integrity (52, 53). By this model, proteins that shape the OM support assembly of the pump complex and thereby resilience in the presence of drug. Overall, the targets revealed by this work indicate that the FQR pump hyper-expressers are more vulnerable to changes in the OM composition than strains lacking these pumps. Components that support the integrity of the permeability barrier and stabilize RND drug transporters are likely to be important for survival during drug treatment. Consistent with these results is the demonstration that RND pump overexpressing strains are hypersensitive to ZOS and COL, and another previously tested compound, all of which disrupt the OM (49).

In addition to targets linked to OM biogenesis, a pair of loci were identified that had no clear connection to supporting envelope integrity. IhfB is part of the heterodimeric integration host factor complex that is nucleoid-associated and can locally and globally modulate chromosome structure and influence gene expression (38-41). Depletion of IhfB resulted in reduced expression of *adeG* accompanied by increased expression of the pump regulator gene *adeL*, consistent with low pump concentrations leading to CIP sensitization. Although it is unclear how a deficit in IhfB causes this defect, this result opens the door to targeting global regulators as a strategy for combatting drug resistance. The other sensitization locus not easily linked to OM dysfunction was PhaF, which is part of the monovalent cation/proton antiporter

PhaACDEFG complex (54-56). The antiporter may function to control ion or pH homeostasis in the FQR strains to compensate for increased drug-proton antiport activity of the RND efflux pumps. In its absence, there may be suboptimal functioning of the AdeFGH pump leading to increased drug susceptibility.

We also identified that strains depleted of inner membrane-associated F_1F_0 ATPase/synthase subunits (*atpI*, *atpF* in all FQR strains; multiple other *atp* genes in GPL) and of translation-associated factors (*fmt*, *rimM*, *der/engA*, *rnpA*) enhanced fitness of the pump hyper-expressers in CIP. AtpF encodes the ATPase B subunit that connects the F_1 catalytic domain to the F_0 membrane-spanning proton translocator, linking proton translocation to ATP generation by F_1 (44, 45). AtpI, on the other hand, functions as a poorly conserved non-structural chaperone, supporting the formation of the F_0 c-ring and complex stability (57, 58). Depletion of the specific subset of components leading to drug tolerance may be a consequence of their limited lethality after depletion as compared to other components.

There are two clear models for how depletion of F_1F_0 ATP synthase components could provide a fitness advantage in the presence of the drug. First, lowering the cytosolic pH could simply reduce the efficacy of the antibiotic (59, 60). Secondly, similar to the F_1F_0 ATP synthase, RND pumps utilize the proton motive force generated by the electron transport chain, and reducing ATPase synthase concentrations on the membrane may facilitate kinetic linkage of the efflux pump to the respiratory chain. This model is consistent with our previous observation that there were significantly reduced numbers of viable transposon insertion disruptions in the cytochrome b_o (3) ubiquinol oxidase complex in the GPL strain (16). Therefore, the oxidase complex could provide the protons necessary for efflux pump activity. In fact, depletion of the ubiquinol oxidase complex as well as other systems involving the electron transport chain

reduced fitness of GPN and GPL even in the absence of drug in this study, indicating that the oxidase may play an important homeostatic role even in the absence of known substrates (Supp. Fig. 5E). Therefore, the ATP synthase and the ubiquinol oxidase appear to play opposing roles in supporting fitness of pump overproducing strains.

Interestingly, in our RNA-seq experiments, we found that *atpE* transcription was significantly downregulated in the GPL efflux overproducer when compared to the GP strain grown in the absence of drug (16). Although depletion of this critical F_0 component was not shown to protect from drug action, it does emphasize the similarity between drug stress and stress related to overproduction of the AdeFGH pump. Manipulation of the proton motive force may be a critical determinant in protecting against both pump overproduction and drug exposure.

The ATP synthase depletion phenotype after CIP treatment mirrors that of depletions of translation apparatus components, which also result in increased fitness. Perhaps allowing efflux overproducers to enter an ATP-depleted state of dormancy protects against both pump overproduction and drug stress, and this is mirrored by translational disruption. Both lowered ATP and reduced translation have been associated with persister cell formation, allowing bacteria to tolerate stress experienced during drug treatment (61, 62). Interestingly, pump hyperexpression has also been documented to contribute to the development of persistence (63), most notably in the case of the AdeFGH efflux pump (64). Therefore, either depressed ATP synthesis or translation could support the fitness of pump overexpressing isolates, allowing survival in the presence of high antibiotic levels, compensating for stress imparted by elevated levels of transporter. This may be one factor in explaining why translation inhibitors have occasionally been linked to antagonism of fluoroquinolone action (62, 65-68). Future efforts will be directed to exploring these hypotheses in hopes of better understanding the hidden

susceptibilities of pump over-expression and identifying proteins that help support the viability of the MDR state.

Acknowledgements

This work is supported by NIAID grants U01AI124302, U19AI158076, R21AI128328, and U19AI142780. We thank Megan W. Tse (Broad Institute of Massachusetts Institute of Technology and Harvard) for LptC and LptG hypomorphs, Defne Surujon (Boston College) for a sam-to-wig file conversion script, Yunfei Dai (Northeastern University) for communications regarding dCas9 strain generation, sgRNA design, and TRANSIT, and for the pYDE009 and pYDE007 plasmids, Rebecca Batorsky (Tufts Technology Services) for aiding with TRANSIT accessibility, and Albert Tai (Tufts Genomics Core Facility) for communications regarding sequencing and library preparation.

R.R.I and E.H conceptualized and devised the study. E.H and W.H designed the sgRNA library. E.H, K.N, and I.N ran the preliminary screens with WT and GPS in the absence of drug. E.H executed the CIP screen and hit validations. W.H tested depletion efficiency of select high fitness perfect sgRNAs, provided bioinformatic support, and reviewed the manuscript. E.G shared all strains, vectors, and methodologies for CRISPRi set up and edited the manuscript. E.H and R.R.I interpreted the results and wrote the manuscript.

Materials and Methods

Bacterial strains and growth conditions. Bacterial strains used in this work are listed in Supplementary Data 1. All *Acinetobacter baumannii* strains are derived from ATCC 17978UN. Cultures were grown in lysogeny broth (LB) (10 g/L tryptone, 5 g/L yeast extract, 10 g/L NaCl) or on LB agar plates (LB supplemented with 15g/L agar. Superoptimal broth with catabolite repression (SOC) was used for recovery following all electroporations of *A. baumannii*. Electroporations were performed using 0.1cm gap cuvettes and Bio Rad Gene Pulser, with the settings 200 Ω, 25 µF, and 1.8 kV. For growth in broth culture, bacteria were aerated at 37°C on a platform shaker, roller drum, or shaking in 96-well plates (Costar) with growth monitored by measuring absorbance via a spectrophotometer at 600nm (A_{600}) with Genesys 30 (Thermo Scientific) or Epoch 2 or SynergyMx (Biotek) plate readers. Cultures were first incubated to early post-exponential phase in LB before diluted to a starting A_{600} of 0.003 in 5mL LB broth or in 200µl LB (96-well plates) supplemented with aTc for dCas9 induction (when hypomorphs are evaluated) and drug where applicable. Growth was monitored every 15 minutes (plate reader) or evaluated after 170min (dCas9 induced but not drug treated) and 230min (dCas9 induced and drug treated). LB was supplemented with antibiotics, as needed, at the following concentrations: aTc: 100ng/mL, Carbenicillin (Carb): 50/100µg/mL, Gentamicin (Gent): 10µg/mL, Chloramphenicol (Cm): 10/25µg/mL, VANC: 64 µg/mL, SDS: 0.05%, COL: 0.2µg/mL, CIP: varying concentrations (Sigma), or ZOS: 2.5µm (MedChemExpress).

Molecular cloning and mutant construction. Primers (IDT or GENEWIZ) and plasmids used throughout this study are listed in Supplementary Data 1. The dCas9 construction is tetracycline (Tet)-inducible and chromosomally embedded at the Tn7 site in the four strains of interest. The plasmids and techniques used to create these strains are as previously described (23,

28). Briefly, the mobile Tet-inducible dCas9 was introduced into the four *A. baumannii* recipient strains of interest via four parental mating and Tn7 transposition. The recipient *A. baumannii* strains, the HB101 RK600Cm^{R} helper, EGE187 DH5α λpir (pTNS3) encoding the T7 transposase, and the YDE009 DH5α (pUC18T-miniTn7T-GentR with *tetR-P*$_{Tet}$*::dCas9-rrnB*T1-T7Te) donor strain were grown overnight in LB with appropriate antibiotics. The following day the cultures were normalized to A_{600} of 2.0 and 100µl of each of the three *E. coli* cultures were combined with 100µl of each *A. baumannii* recipient culture in 600µl LB, prewarmed to 37°C. The mixture was washed twice in 37°C LB, then resuspended in 25µl of fresh broth and spotted on pre-warmed LB agar plates. These plates were incubated at 37°C for approximately 5 hours then resuspended in 1mL sterile phosphate buffered saline (PBS) before plating and overnight selection on Vogel-Bonner minimal medium (VBM) containing 10µg/mL of Gent to select against *E. coli* strains and the parental Gent^{S} *A. baumannii*. Exconjugants were colony-purified on VBM containing 10µg/mL Gent, and screened on LB agar with 100µg/mL Carb and on LB agar with 10µg/mL Gent. The insertion at the *att*Tn7 site downstream the *glmS* gene was confirmed by colony PCR using the primers glmS2-F1 and Tn7R-R1.

The vector pYDE007 used to introduce the sgRNAs is a shuttle plasmid previously described (23) containing the origin of replication of pBR322 and an origin of replication from a natural *Acinetobacter* isolate pWH1277 (23) to allow for propagation in both *E. coli* and *A. baumannii* respectively. It encodes for the β-lactamase gene (*bla*) on the backbone and contains a sequence to be replaced by an sgRNA sequence upstream of the dCas9 handle and *S. pyogenes* transcriptional terminator, with the fusion driven by the constitutive synthetic promoter pJ23119. For efficient cloning of sgRNAs, the vector was made GoldenGate^{TM}-compatible by first mutating the single BsaI Type II restriction site present in the *bla* gene and then introducing two

BsaI sites between the promoter and dCas9 handle to allow for directional sgRNA oligo insertion. Using this backbone, all 24nt sgRNA oligos were constructed with additional 4nt overhangs that allowed for directional cloning. The sgRNA bank was designed by loosely following a previous strategy for stoichiometric knockdowns (17), and the vector and library design were used for construction of the sgRNA-plasmid library by contract (GENEWIZ).

Identification of essential genes in *Acinetobacter baumannii*. Essential genes of *A. baumannii* ATCC 17978UN were determined using transposon mutagenesis sequence data in the WT strain (16, 22), and the data from that study was subjected to TRANSIT Gumbel analysis to identify the essential genes (23-25). Briefly, sequence mapped SAM files were converted to wig files with a custom python script bowtie_to_wig2.py provided by Defne Surujon from the Tim van Opijnen lab. The wig files were then used as input, using the TRANSIT Gumbel analysis pipeline (25) with default settings. Cross referencing our list of essential genes to those similarly identified in other studies in the same strain or the more recently isolated AB5075 clinical strain revealed 406 genes exhibiting a high likelihood of essentiality, given their classification as essential in at least one of the other published analyses as well (23, 26, 27).

sgRNA library design. The 24nt sgRNAs were principally designed (to target each essential gene) with the antisense strand sequence using a PAM site on the antisense strand that is as close as possible to the translational start site. The sgRNA pool was then expanded with an additional 23 mismatch sgRNAs that differ from each targeting sgRNA by 1 or 2 nts, along with 5 shuffle sgRNAs that comprise the same nts as the original target-homologous sgRNA but are shuffled to minimize the likelihood of off-target effects. An additional 216 “pool shuffle” sgRNAs of an array of nts with the GC content of the targeted genes designed to minimize homology to any genomic sequence, bringing the final sgRNA pool to 12,000 sgRNAs total

(Supp. Data 2). Mismatches were employed to introduce sgRNAs with reduced knockdown efficiencies, while the shuffles served as negative controls (anticipated to provide a neutral effect on fitness). A BLAST search did reveal that up to 12bp overlap with the genome was unavoidable among some members of the control pool. These mismatches and shuffle sgRNAs were designed as previously described (17), using the python script 'final sgRNA dirty pool design.ipynb' (accessible via GitHub: https://github.com/isberglab/CRISPRiaDesign.git).

Preparation of pools with sgRNA library. The sgRNA-pDNA library was introduced into the FQR pump hyper-expressers and WT strain with chromosomally encoded Tet-inducible dCas9 via electroporation. About 50µl electrocompetent cells were transformed with 23-46ng of the pDNA, the resuspended mixture diluted 1/10, and 200µl plated on five large pre-warmed SOC agar plates overlain with mixed cellulose ester filters (0.45µm pore size, 137mm diameter, Advantec). The mixture was spread on the filters using beads. This was repeated for a total of 3 transformations per strain background. These transformants were allowed to recover at 37°C for an hour on SOC agar plates before the filters were transferred to selective LB agar plates containing 50µg/mL Carb and incubated overnight at 37°C for about 13.5-14 hours. The following day, filters were pooled to acquire somewhere around 250,000-350,000 CFUs, estimated based on using image analysis of previous pools (ImageJ). Pooling entailed washing colonies off with 100mL sterile PBS with gentle shaking in a sterile round bottom 3L beaker. Glycerol was added to a final concentration of 10-20% and 1mL aliquots were placed into cryotubes for -80°C storage until needed.

Identification of hypomorphs with fitness defects. Following previous protocols for determining fitness using Tn-Seq pools (10, 22), each vial of *A. baumannii* P_{Tet}*::dCas9* harboring the sgRNA array was thawed on ice, diluted into 25mL LB to an A_{600}=0.1, and revived

by incubation at 37°C with shaking for 50min-60min until they reached around A_{600}=0.2. Each culture was then diluted to an A_{600}=0.003 in 10mL LB in the absence or presence of 100ng/mL aTc for dCas9 induction and the fluoroquinolone CIP. Cultures were incubated for approximately 7-8 generations on the drum wheel at 37°C, for about 170 (no drug treatment) or 230 (CIP treated) minutes, until densities reached A_{600}= 0.5-0.895. The cultures were harvested both before (T1) and after (T2) dCas9 induction and drug treatment to allow sgRNA fitness analyses. Sample pellets were stored at -20°C until all were collected. Plasmid was extracted from each sample using the QIAprep Spin Miniprep Kit (Qiagen) following manufacturer's protocol.

sgRNAs were amplified from harvested plasmid DNA using primers For2_sgRNA_Pool and Rev_sgRNA_Pool at 0.6µM in a 50µl PCR reaction with 10µl 5x Q5 buffer, 0.5µl of Q5 hot start polymerase, 1µl 100mM dNTPs (NEB), 100ng of the pDNA, and UltraPure water (Thermo Fisher Scientific). The thermocycler settings were as follows with a heated lid: 98°C for 1min, 14 cycles of 98°C for 10sec, 70°C for 20sec, and 72°C for 1min, then finally 72°C for 2min. Barcodes were then introduced with a second round PCR using a legacy Nextera kit of adaptors (Illumina, compatible with FC-121-1031, FC-121-1030, FC-121-1012, FC-121-1011). The second PCR was performed using 1µl of the first PCR product, 4µl UltraPure water, 7.5µl 2x NEBNext High Fidelity Master Mix (NEB), and 1.25µl of each barcoded Nextera N5x and N7x index primers per reaction. The thermocycler was set up to hold a heated lid while running at 72°C for 3min, 98°C for 2:45min, and 8 cycles of 98°C for 15sec, 65°C for 30sec, and 72°C for 1:30min. The desired amplified product is 328nt in length. 5µl samples of the PCR2 products were fractionated on a 2% agarose Tris-Acetate-EDTA (TAE) gel using Sybr Safe dye (Invitrogen) alongside a set amount of 100bp DNA ladder (NEB) and run for 1hr at about 90V

for quantification. Samples were imaged and concentrations measured using a BioRad quantitative gel doc system, with quantitation performed using Image J, or dedicated Bio-Rad software so that approximately 100ng of each sample was pooled for sequencing. The samples were PCR column purified (Qiagen) and their final concentrations determined via Nanodrop prior to submission to Tufts University Core Facility of Genomics for sequencing. The pools were sequenced via Illumina HiSeq 2500 SE100 using a legacy Nextera primer mixture.

The 5' sequence preceding the 24nt sgRNA was trimmed using Cutadapt (69). Reads were assigned to each sgRNA using a Python script as described (18). To better assess fitness of all hypomorphs in the pool, a set of 25 shuffle sgRNAs were chosen to serve as negative/neutral controls: The dataset used was from a preliminary study comprising 10 replicate cultures from the WT and GPS strains harboring the sgRNA library grown in rich media in the presence or absence of dCas9 induction. To identify the neutral controls, the assigned reads for all sgRNAs at T1 and at T2, in the induced and uninduced cultures in each strain background, were normalized to the total reads in each replicate sample and then transformed by 1x10^6. As there were 10 replicates per condition, these values were averaged across replicates for each sgRNA. The median was then determined for each condition and the sgRNAs falling within the 25-75th percentile were identified. Shuffle sgRNAs that fell in this range across all conditions in both the WT and GPS strain backgrounds were identified as candidates for the normalization controls. Among these sgRNAs were a set of guides that also yielded mean fitness values within the 25th-75th percentile in more than one condition, 25 of which were selected as neutral controls for downstream fitness normalization.

To calculate fitness of all hypomorphs screened in the pool, read counts for each sgRNA were first normalized to the total assigned reads per sample. Any counts of 0 were given a read

count of 1 for downstream fitness calculations. Fitness yields from each sgRNA were determined as described (29, 70). Fitness values were then normalized to the set of 25 shuffle sgRNAs serving as neutral controls by dividing each individual sgRNA fitness score by the average fitness of those 25 sgRNAs in each sample. Normalized fitness values of each sgRNA were then compared as described in Results. Multiple unpaired t-test analysis was used to identify significant differences in fitness as a consequence of drug treatment or strain background. Discoveries of fitness scores that significantly differ in these comparisons were determined by the two-stage step-up method of Benjamini, Krieger, and Yekutieli with Q < 5% (30). Findings characterized as top discoveries were targets represented by 3 or more sgRNAs. Those with <10 cumulative reads across replicate cultures at T1 prior to outgrowth as well as ribosomal genes were excluded. Data pertaining to the CIP screen are shown in Supplementary Data 4. All sequence data is also deposited in the SRA database under BioProject number PRJNA1067098.

Validation of individual CRISPRi fitness defects. Individual sgRNA vectors were constructed by digestion of the pEHE51 vector with BsaI-HFv2 (NEB) prior to gel extraction followed by guide oligonucleotide insertion. The 24nt oligonucleotide guides (1µl of each complementary oligo at 100µM) containing 4nt overhangs were incubated with T4 PNK (NEB) for 1.5hrs at 37°C, followed by addition of 2µl 1M NaCl and oligo annealing starting at 95°C, with ramping to 25°C performed using a temperature drop of 15-20°C every 5min. Oligos were diluted 100X and 4µl were ligated to 100ng vector with T4 DNA Ligase (NEB) overnight at 16°C prior to electroporation into dCas9-harboring strains. Individual hypomorphs were tested by growth to early post-exponential phase in LB, followed by dilution to A_{600}~0.003 in LB supplemented with 100ng/mL of aTc with or without CIP (at varying concentrations) and

641 measuring A_{600} at 170 min (untreated) or 230 min (CIP treated). Doubling times were
642 determined ($Time_{min}$ x Log(2))/(Log($A_{600@T2}$)-Log($A_{600@T1}$)).

643 **pHi Assay.** This assay was performed as previously described (16). To note, the
644 hypomorphs (and shuffle controls) evaluated in this work were grown to late exponential phase
645 before dilution to A_{600} of 0.01 or 0.003 in LB + 100ng/mL aTc. These cultures were incubated to
646 mid-exponential growth phase without additional drug (Untx) or to mid-exponential growth
647 phase then with CIP 60 µg/mL added for an additional hour. Bacteria were harvested
648 (approximately A_{600} ~2-3.5), 1/5th diluted in 20µM BCECF-AM (Thermo Fisher Scientific) in
649 PBS and incubated for 30min at 30°C. 50-100µl (1/4th or 1/8th) was pelleted and energized in LB
650 for 5min at 37°C, followed by re-suspension 1:1 (1/2 diluted) in mixed dibasic sodium phosphate
651 and monosodium phosphate buffer of varying pH (standard curve to which 10µM CCCP is
652 added) or neutral pH (experimental samples) for downstream pHi evaluation.

653 **qRT-PCR.** Cultures were grown in LB broth to early post-exponential phase before
654 dilution into 5mL LB with 100ng/mL aTc to a starting A_{600} of 0.003 (0.01 in 3mL for AtpF
655 depletion). Cultures were harvested after 170min reaching A_{600} of 0.134 to 0.904 (average
656 0.466). The following steps are as previously described (16): RNA was extracted using RNeasy
657 (Qiagen). RNA was treated with ezDNase before cDNA synthesis with the SuperScript VILO
658 cDNA kit (Thermo Fisher). Targets were amplified using PowerUp SYBR Green Master Mix
659 (Applied Biosystems) and CT values determined using the StepOnePlus Real-Time PCR system
660 (Applied Biosystems). The efficiency of primer pairs used for target amplification was evaluated
661 using a standard curve of cDNA at varying dilutions and consequently verified to be about 94-
662 108% for each pair used. Three biological replicates were evaluated for each strain or
663 hypomorph and three technical replicates examined per biological sample during target

amplification. To test for gDNA contamination, a set of control samples were tested in parallel which were not reverse transcribed during the cDNA synthesis reactions. Transcript levels of each specified target were compared between each hypomorph and the control strain harboring a non-targeting shuffle sgRNA, NC_159, after normalization to levels of 16S.

References

1. CDC. 2019. Antibiotic Resistance Threats in the United States. Atlanta, GA: US Department of Health and Human Services, CDC.
2. CDC. 2022. COVID-19: U.S. Impact on Antimicrobial Resistance, Special Report 2022. Atlanta, GA: US Department of Health and Human Services, CDC.
3. Tacconelli E, Carrara E, Savoldi A, Harbarth S, Mendelson M, Monnet DL, Pulcini C, Kahlmeter G, Kluytmans J, Carmeli Y, Ouellette M, Outterson K, Patel J, Cavaleri M, Cox EM, Houchens CR, Grayson ML, Hansen P, Singh N, Theuretzbacher U, Magrini N, Group WHOPPLW. 2018. Discovery, research, and development of new antibiotics: the WHO priority list of antibiotic-resistant bacteria and tuberculosis. Lancet Infect Dis 18:318-327.
4. Sun J, Deng Z, Yan A. 2014. Bacterial multidrug efflux pumps: mechanisms, physiology and pharmacological exploitations. Biochem Biophys Res Commun 453:254-67.
5. Poole K. 2004. Efflux-mediated multiresistance in Gram-negative bacteria. Clin Microbiol Infect 10:12-26.
6. Coyne S, Courvalin P, Perichon B. 2011. Efflux-mediated antibiotic resistance in *Acinetobacter* spp. Antimicrob Agents Chemother 55:947-53.

7. Pagdepanichkit S, Tribuddharat C, Chuanchuen R. 2016. Distribution and expression of the Ade multidrug efflux systems in *Acinetobacter baumannii* clinical isolates. Can J Microbiol 62:794-801.

8. Rumbo C, Gato E, Lopez M, Ruiz de Alegria C, Fernandez-Cuenca F, Martinez-Martinez L, Vila J, Pachon J, Cisneros JM, Rodriguez-Bano J, Pascual A, Bou G, Tomas M, Spanish Group of Nosocomial I, Mechanisms of A, Resistance to A, Spanish Society of Clinical M, Infectious D, Spanish Network for Research in Infectious D. 2013. Contribution of efflux pumps, porins, and beta-lactamases to multidrug resistance in clinical isolates of *Acinetobacter baumannii*. Antimicrob Agents Chemother 57:5247-57.

9. Fernando D, Zhanel G, Kumar A. 2013. Antibiotic resistance and expression of resistance-nodulation-division pump- and outer membrane porin-encoding genes in *Acinetobacter* species isolated from Canadian hospitals. Can J Infect Dis Med Microbiol 24:17-21.

10. Geisinger E, Vargas-Cuebas G, Mortman NJ, Syal S, Dai Y, Wainwright EL, Lazinski D, Wood S, Zhu Z, Anthony J, van Opijnen T, Isberg RR. 2019. The Landscape of Phenotypic and Transcriptional Responses to Ciprofloxacin in *Acinetobacter baumannii*: Acquired Resistance Alleles Modulate Drug-Induced SOS Response and Prophage Replication. mBio 10.

11. Naidu V, Bartczak A, Brzoska AJ, Lewis P, Eijkelkamp BA, Paulsen IT, Elbourne LDH, Hassan KA. 2023. Evolution of RND efflux pumps in the development of a successful pathogen. Drug Resist Updat 66:100911.

12. Magnet S, Courvalin P, Lambert T. 2001. Resistance-nodulation-cell division-type efflux pump involved in aminoglycoside resistance in *Acinetobacter baumannii* strain BM4454. Antimicrob Agents Chemother 45:3375-80.

13. Coyne S, Rosenfeld N, Lambert T, Courvalin P, Perichon B. 2010. Overexpression of resistance-nodulation-cell division pump AdeFGH confers multidrug resistance in *Acinetobacter baumannii*. Antimicrob Agents Chemother 54:4389-93.

14. Yoon EJ, Chabane YN, Goussard S, Snesrud E, Courvalin P, De E, Grillot-Courvalin C. 2015. Contribution of resistance-nodulation-cell division efflux systems to antibiotic resistance and biofilm formation in *Acinetobacter baumannii*. mBio 6.

15. Rosenfeld N, Bouchier C, Courvalin P, Perichon B. 2012. Expression of the resistance-nodulation-cell division pump AdeIJK in *Acinetobacter baumannii* is regulated by AdeN, a TetR-type regulator. Antimicrob Agents Chemother 56:2504-10.

16. Hamami E, Huo W, Hernandez-Bird J, Castaneda A, Bai J, Syal S, Ortiz-Marquez JC, van Opijnen T, Geisinger E, Isberg RR. 2025. Identification of determinants that allow maintenance of high-level fluoroquinolone resistance in *Acinetobacter baumannii*. mBio 16:e0322124.

17. Jost M, Santos DA, Saunders RA, Horlbeck MA, Hawkins JS, Scaria SM, Norman TM, Hussmann JA, Liem CR, Gross CA, Weissman JS. 2020. Titrating gene expression using libraries of systematically attenuated CRISPR guide RNAs. Nat Biotechnol 38:355-364.

18. Hawkins JS, Silvis MR, Koo BM, Peters JM, Osadnik H, Jost M, Hearne CC, Weissman JS, Todor H, Gross CA. 2020. Mismatch-CRISPRi Reveals the Co-varying Expression-Fitness Relationships of Essential Genes in *Escherichia coli* and *Bacillus subtilis*. Cell Syst 11:523-535 e9.

19. Rousset F, Cui L, Siouve E, Becavin C, Depardieu F, Bikard D. 2018. Genome-wide CRISPR-dCas9 screens in *E. coli* identify essential genes and phage host factors. PLoS Genet 14:e1007749.

20. Ward RD, Tran JS, Banta AB, Bacon EE, Rose WE, Peters JM. 2024. Essential gene knockdowns reveal genetic vulnerabilities and antibiotic sensitivities in *Acinetobacter baumannii*. mBio 15:e0205123.

21. Tran JS, Ward RD, Iruegas-Lopez R, Ebersberger I, Peters JM. 2025. Chemical genomics informs antibiotic and essential gene function in *Acinetobacter baumannii*. PLoS Genet 21:e1011642.

22. Geisinger E, Mortman NJ, Dai Y, Cokol M, Syal S, Farinha A, Fisher DG, Tang AY, Lazinski DW, Wood S, Anthony J, van Opijnen T, Isberg RR. 2020. Antibiotic susceptibility signatures identify potential antimicrobial targets in the *Acinetobacter baumannii* cell envelope. Nat Commun 11:4522.

23. Bai J, Dai Y, Farinha A, Tang AY, Syal S, Vargas-Cuebas G, van Opijnen T, Isberg RR, Geisinger E. 2021. Essential Gene Analysis in *Acinetobacter baumannii* by High-Density Transposon Mutagenesis and CRISPR Interference. J Bacteriol 203:e0056520.

24. DeJesus MA, Ambadipudi C, Baker R, Sassetti C, Ioerger TR. 2015. TRANSIT--A Software Tool for Himar1 TnSeq Analysis. PLoS Comput Biol 11:e1004401.

25. DeJesus MA, Zhang YJ, Sassetti CM, Rubin EJ, Sacchettini JC, Ioerger TR. 2013. Bayesian analysis of gene essentiality based on sequencing of transposon insertion libraries. Bioinformatics 29:695-703.

26. Gallagher LA, Ramage E, Weiss EJ, Radey M, Hayden HS, Held KG, Huse HK, Zurawski DV, Brittnacher MJ, Manoil C. 2015. Resources for Genetic and Genomic Analysis of Emerging Pathogen *Acinetobacter baumannii*. J Bacteriol 197:2027-35.

27. Wang N, Ozer EA, Mandel MJ, Hauser AR. 2014. Genome-wide identification of *Acinetobacter baumannii* genes necessary for persistence in the lung. mBio 5:e01163-14.

28. Peters JM, Koo BM, Patino R, Heussler GE, Hearne CC, Qu J, Inclan YF, Hawkins JS, Lu CHS, Silvis MR, Harden MM, Osadnik H, Peters JE, Engel JN, Dutton RJ, Grossman AD, Gross CA, Rosenberg OS. 2019. Enabling genetic analysis of diverse bacteria with Mobile-CRISPRi. Nat Microbiol 4:244-250.

29. van Opijnen T, Bodi KL, Camilli A. 2009. Tn-seq: high-throughput parallel sequencing for fitness and genetic interaction studies in microorganisms. Nat Methods 6:767-72.

30. Benjamini Y, Krieger, A. M., & Yekutieli, D. 2006. Adaptive linear step-up procedures that control the false discovery rate. Biometrika 93:491-507.

31. Yakhnin AV, Bubunenko M, Mandell ZF, Lubkowska L, Husher S, Babitzke P, Kashlev M. 2023. Robust regulation of transcription pausing in *Escherichia coli* by the ubiquitous elongation factor NusG. Proc Natl Acad Sci U S A 120:e2221114120.

32. Baniulyte G, Singh N, Benoit C, Johnson R, Ferguson R, Paramo M, Stringer AM, Scott A, Lapierre P, Wade JT. 2017. Identification of regulatory targets for the bacterial Nus factor complex. Nat Commun 8:2027.

33. Leus IV, Weeks JW, Bonifay V, Smith L, Richardson S, Zgurskaya HI. 2018. Substrate Specificities and Efflux Efficiencies of RND Efflux Pumps of *Acinetobacter baumannii*. J Bacteriol 200.

34. Sugawara E, Nikaido H. 2014. Properties of AdeABC and AdeIJK efflux systems of *Acinetobacter baumannii* compared with those of the AcrAB-TolC system of *Escherichia coli*. Antimicrob Agents Chemother 58:7250-7.

35. Raskin DM, Judson N, Mekalanos JJ. 2007. Regulation of the stringent response is the essential function of the conserved bacterial G protein CgtA in *Vibrio cholerae*. Proc Natl Acad Sci U S A 104:4636-41.

36. Diez S, Ryu J, Caban K, Gonzalez RL, Jr., Dworkin J. 2020. The alarmones (p)ppGpp directly regulate translation initiation during entry into quiescence. Proc Natl Acad Sci U S A 117:15565-15572.

37. Pahil KS, Gilman MSA, Baidin V, Clairfeuille T, Mattei P, Bieniossek C, Dey F, Muri D, Baettig R, Lobritz M, Bradley K, Kruse AC, Kahne D. 2024. A new antibiotic traps lipopolysaccharide in its intermembrane transporter. Nature 625:572-577.

38. Chen S, Hu M, Hu A, Xue Y, Wang S, Liu F, Li C, Zhou X, Zhou J. 2022. The integration host factor regulates multiple virulence pathways in bacterial pathogen *Dickeya zeae* MS2. Mol Plant Pathol 23:1487-1507.

39. Fan Z, Fu T, Li Z, Du B, Cui X, Zhang R, Feng Y, Zhao H, Xue G, Cui J, Yan C, Gan L, Feng J, Xu Z, Yu Z, Tian Z, Ding Z, Chen J, Chen Y, Yuan J. 2023. The role of integration host factor in biofilm and virulence of high-alcohol-producing *Klebsiella pneumoniae*. Microbiol Spectr 11:e0117023.

40. Nicolau SE, Lewis K. 2022. The Role of Integration Host Factor in *Escherichia coli* Persister Formation. mBio 13:e0342021.

41. Friedman DI. 1988. Integration host factor: a protein for all reasons. Cell 55:545-54.

42. Sielaff H, Duncan TM, Borsch M. 2018. The regulatory subunit epsilon in *Escherichia coli* F(O)F(1)-ATP synthase. Biochim Biophys Acta Bioenerg 1859:775-788.

43. Guo H, Courbon GM, Bueler SA, Mai J, Liu J, Rubinstein JL. 2021. Structure of mycobacterial ATP synthase bound to the tuberculosis drug bedaquiline. Nature 589:143-147.

44. Saw WG, Le KCM, Shin J, Kwek JHM, Wong CF, Ragunathan P, Fong TC, Muller V, Gruber G. 2023. Atomic insights of an up and down conformation of the *Acinetobacter baumannii* F(1) -ATPase subunit epsilon and deciphering the residues critical for ATP hydrolysis inhibition and ATP synthesis. FASEB J 37:e23040.

45. Demmer JK, Phillips BP, Uhrig OL, Filloux A, Allsopp LP, Bublitz M, Meier T. 2022. Structure of ATP synthase from ESKAPE pathogen *Acinetobacter baumannii*. Sci Adv 8:eabl5966.

46. Xu Q, Guo M, Yu F. 2023. beta-Barrel Assembly Machinery (BAM) Complex as Novel Antibacterial Drug Target. Molecules 28.

47. Sklar JG, Wu T, Kahne D, Silhavy TJ. 2007. Defining the roles of the periplasmic chaperones SurA, Skp, and DegP in *Escherichia coli*. Genes Dev 21:2473-84.

48. Fenn KL, Horne JE, Crossley JA, Bohringer N, Horne RJ, Schaberle TF, Calabrese AN, Radford SE, Ranson NA. 2024. Outer membrane protein assembly mediated by BAM-SurA complexes. Nat Commun 15:7612.

49. Tse MW, Zhu M, Peters B, Hamami E, Chen J, Davis KP, Nitz S, Weller J, Warrier T, Hunt DK, Morales Y, Kawate T, Gaulin JL, Come JH, Hernandez-Bird J, Huo W, Neisewander I, Yu X, Aceves-Salvador JA, Kiessling LL, Hung DT, Mecsas J, Aldridge BB, Isberg RR, Blainey PC. 2025. Large-scale combination screens reveal small-

molecule sensitization of antibiotic-resistant gram-negative ESKAPE pathogens. Proc Natl Acad Sci U S A 122:e2402017122.

50. Ruiz N, Gronenberg LS, Kahne D, Silhavy TJ. 2008. Identification of two inner-membrane proteins required for the transport of lipopolysaccharide to the outer membrane of *Escherichia coli*. Proc Natl Acad Sci U S A 105:5537-42.

51. Sperandeo P, Cescutti R, Villa R, Di Benedetto C, Candia D, Deho G, Polissi A. 2007. Characterization of lptA and lptB, two essential genes implicated in lipopolysaccharide transport to the outer membrane of *Escherichia coli*. J Bacteriol 189:244-53.

52. Arunmanee W, Pathania M, Solovyova AS, Le Brun AP, Ridley H, Basle A, van den Berg B, Lakey JH. 2016. Gram-negative trimeric porins have specific LPS binding sites that are essential for porin biogenesis. Proc Natl Acad Sci U S A 113:E5034-43.

53. Webby MN, Oluwole AO, Pedebos C, Inns PG, Olerinyova A, Prakaash D, Housden NG, Benn G, Sun D, Hoogenboom BW, Kukura P, Mohammed S, Robinson CV, Khalid S, Kleanthous C. 2022. Lipids mediate supramolecular outer membrane protein assembly in bacteria. Sci Adv 8:eadc9566.

54. Dzioba-Winogrodzki J, Winogrodzki O, Krulwich TA, Boin MA, Hase CC, Dibrov P. 2009. The *Vibrio cholerae* Mrp system: cation/proton antiport properties and enhancement of bile salt resistance in a heterologous host. J Mol Microbiol Biotechnol 16:176-86.

55. Ito M, Guffanti AA, Wang W, Krulwich TA. 2000. Effects of nonpolar mutations in each of the seven *Bacillus subtilis* mrp genes suggest complex interactions among the gene products in support of Na(+) and alkali but not cholate resistance. J Bacteriol 182:5663-70.

56. Kosono S, Haga K, Tomizawa R, Kajiyama Y, Hatano K, Takeda S, Wakai Y, Hino M, Kudo T. 2005. Characterization of a multigene-encoded sodium/hydrogen antiporter (sha) from *Pseudomonas aeruginosa*: its involvement in pathogenesis. J Bacteriol 187:5242-8.

57. Koumandou VL, Kossida S. 2014. Evolution of the F0F1 ATP synthase complex in light of the patchy distribution of different bioenergetic pathways across prokaryotes. PLoS Comput Biol 10:e1003821.

58. Liu J, Hicks DB, Krulwich TA. 2013. Roles of AtpI and two YidC-type proteins from alkaliphilic *Bacillus pseudofirmus* OF4 in ATP synthase assembly and nonfermentative growth. J Bacteriol 195:220-30.

59. Dalhoff A, Stubbings W, Schubert S. 2011. Comparative *In Vitro* Activities of the Novel Antibacterial Finafloxacin against Selected Gram-Positive and Gram-Negative Bacteria Tested in Mueller-Hinton Broth and Synthetic Urine. Antimicrobial Agents and Chemotherapy 55:1814-1818.

60. Dalhoff A, Schubert S, Vente A. 2017. Pharmacodynamics of Finafloxacin, Ciprofloxacin, and Levofloxacin in Serum and Urine against TEM- and SHV-Type Extended-Spectrum-ß-Lactamase-Producing *Enterobacteriaceae* Isolates from Patients with Urinary Tract Infections. Antimicrobial Agents and Chemotherapy 61:10.1128/aac.02446-16.

61. Manuse S, Shan Y, Canas-Duarte SJ, Bakshi S, Sun WS, Mori H, Paulsson J, Lewis K. 2021. Bacterial persisters are a stochastically formed subpopulation of low-energy cells. PLoS Biol 19:e3001194.

62. Shan Y, Brown Gandt A, Rowe SE, Deisinger JP, Conlon BP, Lewis K. 2017. ATP-Dependent Persister Formation in *Escherichia coli*. mBio 8.

63. El Meouche I, Dunlop MJ. 2018. Heterogeneity in efflux pump expression predisposes antibiotic-resistant cells to mutation. Science 362:686-690.

64. Huo W, Busch LM, Hernandez-Bird J, Hamami E, Marshall CW, Geisinger E, Cooper VS, van Opijnen T, Rosch JW, Isberg RR. 2022. Immunosuppression broadens evolutionary pathways to drug resistance and treatment failure during *Acinetobacter baumannii* pneumonia in mice. Nat Microbiol 7:796-809.

65. Bollenbach T, Quan S, Chait R, Kishony R. 2009. Nonoptimal microbial response to antibiotics underlies suppressive drug interactions. Cell 139:707-18.

66. Chait R, Craney A, Kishony R. 2007. Antibiotic interactions that select against resistance. Nature 446:668-71.

67. Cokol M, Kuru N, Bicak E, Larkins-Ford J, Aldridge BB. 2017. Efficient measurement and factorization of high-order drug interactions in *Mycobacterium tuberculosis*. Sci Adv 3:e1701881.

68. Ocampo PS, Lazar V, Papp B, Arnoldini M, Abel zur Wiesch P, Busa-Fekete R, Fekete G, Pal C, Ackermann M, Bonhoeffer S. 2014. Antagonism between bacteriostatic and bactericidal antibiotics is prevalent. Antimicrob Agents Chemother 58:4573-82.

69. Martin M. 2011. Cutadapt removes adapter sequences from high-throughput sequencing reads. 2011 17:3.

70. van Opijnen T, Camilli A. 2013. Transposon insertion sequencing: a new tool for systems-level analysis of microorganisms. Nat Rev Microbiol 11:435-42.

Figure legends

Figure 1: Pooled CRISPRi screen to identify hypomorphs with reduced fitness in FQR strains. Diagram for experimental approach and sgRNA library design (Materials & Methods). sgRNAs were designed to target 406 essential genes in *A. baumannii* ("perfect" guides). For each perfect guide, a set of 23 guides with 1 to 2 mismatched nts were created to achieve titratable knockdown efficiencies as well as 5 sequence-shuffled guides as negative controls. Additional pool shuffle sgRNAs were made to generate a library of 12,000 guides. Cultures were harvested before (T1) and after (T2) outgrowth with or without CIP and the dCas9 inducer aTc. Plasmid was extracted and sequenced to identify hypomorphs with altered fitness under tested conditions. Hypomorph fitness scores, normalized to scrambled guides, were compared between control and experimental groups to determine essential gene targets that generate altered fitness of high-level FQR strains relative to WT in either the presence or absence of CIP. FQR: fluoroquinolone resistant. CIP: ciprofloxacin. Untx: untreated. Ind: dCas9 induced using aTc.

Figure 2: sgRNA fidelity to essential gene sequences and mismatch distance from PAM site correspond with fitness decreases in *A. baumannii* CRISPRi strains. Volcano plots are displayed to show statistical significance as a function of the mean change in fitness scores that result from dCas9 induction (100ng/mL aTc, n=10). All symbols refer to unique sgRNAs (light gray). The horizontal dotted line (A-D): FDR or Q=5%. (A) Displayed are shuffle sgRNAs that serve as negative controls (black). (B) The sgRNAs with perfect sequence identity to their target (black). (C) The sgRNAs with mismatched nts located most proximal to the 3' PAM site (black; nts 23 or 24 of the 24nt sgRNA, -1 or 0 nt from PAM site respectively). (D, E): The sgRNAs designed for *gyrA* (black). S: Shuffle sgRNAs. P: Perfect guide. Positions of mismatched nts in

relation to the 3' PAM site noted, with numbering starting at 0 for the nt immediately upstream the PAM site. (D) Display of mean fitness difference of *gyrA* sgRNAs after induction vs. uninduced. (E) Display of *gyrA* data, showing average fitness scores normalized to fitness in the absence of dCas9 inducer for the perfect sgRNA and sgRNAs with single and double mismatches as well as shuffle sgRNAs (± SEM).

Figure 3: Opposing effects of translation/ATP generation and LOS biogenesis on the fitness of FQR strains relative to WT in the presence of CIP. (A-C) Statistical significance plotted as a function of mean fitness score differences (n=10) between CIP and Untx conditions (top) or FQR and WT strains during CIP treatment (bottom), of the FQR strain backgrounds GPS (A, D), GPN (B, E), or GPL (C, F). Gray: Statistically significant sgRNAs passing the FDR or Q=5% (30). 16 prominent targets from the CIP CRISPRi screen are highlighted. Dotted lines: selection parameters setting fitness shifts by ≥0.2 to identify candidates. CIP: ciprofloxacin treated (50-65µg/mL for the FQR strains or 0.11-0.12µg/mL for WT). Untx: untreated. WT: wildtype. GPS: *gyrAparCadeS*. GPN: *gyrAparCadeN*. GPL: *gyrAparCadeL*.

Figure 4: sgRNAs with minimal effects in the absence of drug that decrease fitness in the presence of CIP. (A) Statistical significance plotted as a function of mean fitness comparing growth in the presence and absence of dCas9 inducer (100ng/mL aTc) for 7-8 generations in the WT strain background (n=10). Gray: all sgRNAs. Blue: sgRNAs displaying neutral fitness effects (scores between -0.05 and 0.05). Red: sgRNAs revealing a fitness enhancement (scores of 0.05 or higher). (B) Heat map of neutral and enhancer sgRNAs (as defined in A) that

significantly diminish FQR fitness in the presence of CIP. These pass the FDR or Q=5% (n=10) via multiple t-test analyses comparing hypomorphs incubated with and without drug (first 4 columns) and between strain backgrounds (FQR-WT) during CIP treatment (last 3 columns). Candidates were considered if at least 3 sgRNAs had fitness score decreased by $\geq$0.095 and at least one sgRNA did so in more than one FQR strain. Gene numbers are originally preceded by "ACX60_" for *A. baumannii* strain ATCC 17978UN (accession NZ_CP012004.1). 0: Perfect sgRNA. FQR: fluoroquinolone resistant. CIP: ciprofloxacin. Untx: untreated. WT: wildtype. GPL: *gyrAparCadeL*. GPN: *gyrAparCadeN*. GPS: *gyrAparCadeS*.

Figure 5: FQR strain hypomorphs that show high fitness levels in the absence of drug and are hypersensitive to CIP affect proteins critical to membrane integrity. (A-H) Statistical significance is plotted as a function of average fitness score differences for hypomorphs comparing dCas9 induced and uninduced conditions (A-D) or comparing CIP and Untx conditions (E-H) in the WT (A, E), GPS (B, F), GPN (C, G), or GPL (D, H) strain backgrounds (n=10). Gray: All sgRNAs. Prominent targets from the screen (7) are highlighted, of which most depletions had little effect on fitness in the absence of drug but showed significantly lowered fitness in the FQR strains during CIP exposure. Dotted lines: selection parameters defining either fitness defect or high fitness. CIP: ciprofloxacin. Untx: untreated. WT: wildtype. GPS: *gyrAparCadeS*. GPN: *gyrAparCadeN*. GPL: *gyrAparCadeL*.

Figure 6: Individual CRISPRi validation assays confirm increased dependence of GPL and GPN strains on LOS biogenesis proteins for growth during CIP stress. (A) Mean fitness

score changes imparted by each sgRNA during CIP exposure as compared to untreated conditions as derived from the CIP CRISPRi pooled screen (n=10). Dotted line represents the mean of scrambled controls that should exert no change in fitness. Light gray: all sgRNAs designed for the listed target (mismatched and shuffled guides included). Data points in red, blue, or orange highlight individual sgRNAs used to validate their respective targets' impact on FQR fitness, as labeled in B. (B-E) These individual sgRNAs were constructed and hypomorphs in all strain backgrounds were cultured in the presence or absence of CIP. Doubling time differences in untreated and CIP treated conditions are superimposed. (B) Mean ± SEM (n=3) growth rates (in min) of hypomorphs are compared to those harboring a shuffle control sgRNA (NC_159). Unpaired t test analyses (individual variance each row) were performed on pre-selected pairs following the two-stage set-up of Benjamini, Krieger, and Yekutieli with a false discovery rate of 5% (30). Significant differences in doubling times yielded by targeted depletions between strains during CIP exposure are shown: *, $p<0.05$; **, $p<0.02$; ***, $p<0.01$; ****, $p<0.001$. (C) Mean ± SEM ($n\geq3$) growth rates are shown (in min) for the listed hypomorphs. Two-way Anova with Tukey's multiple comparisons test reveals significant variations in growth rates between GP and GPL or GPS during CIP exposure: ****, $p<0.0001$. (D) Two-way Anova analyses using pre-selected pairs with Šídák's multiple comparisons test (n=3): **, $p=0.0013$; ***, $p=0.0002$; ****, $p<0.0001$. (E) Mean growth rates (in min) ± SEM (n=3) for hypomorphs growing in the absence or presence of CIP (10 µg/mL for GP and GPLΔ*adeFGH* or 50 µg/mL for GPL) with superimposed values. Statistical significance determined by a two-way Anova with pre-selected pairs and Šídák's multiple comparisons test: ****, $p<0.0001$. CIP: ciprofloxacin (0.1 µg/mL for WT (B), 10 µg/mL (E) or 13 µg/mL (C-D) for GP, 10 µg/mL for GPLΔ*adeFGH* (E), 50 µg/mL for GPS (C), 45 µg/mL for GPN (D), and 50

µg/mL (E) or 60 µg/mL (B-C) for GPL). Untx: untreated. WT: wildtype. GP: *gyrAparC*. GPL: *gyrAparCadeL*. GPN: *gyrAparCadeN*. GPS: *gyrAparCadeS*.

Figure 7: Depletion of LOS and lipoproteins results in defective envelope integrity, but ZOS and COL amplify CIP selectively in the GPL strain. (A-H) Growth of the indicated strains in LB at 37°C is displayed as the mean ± SEM (n≥3) after Y values were log transformed. (A, B) The indicated hypomorphs were grown in the absence of CIP with or without 64 µg/mL VANC (A) or 0.05% SDS (B). (C-H) Strains were incubated in the presence or absence of 2.5µM ZOS (C-E) or COL at 0.2 µg/mL (F-H) together with CIP at 13 µg/mL (C, D), 15 µg/mL (F, G), or 60 µg/mL (E, H). CIP: Ciprofloxacin. ZOS: Zosurabalpin. COL: Colistin. VANC: Vancomycin. SDS: Sodium dodecyl sulfate. GP: *gyrAparC*. GPL: *gyrAparCadeL*.

Figure 8: Non-OM pathways modulating fitness related to pump expression include the IhfB regulator and pH homeostasis. (A) Mean fold change ($2^{-\Delta\Delta CT}$) ± SEM (n=3) in transcript levels of each target in GPL during *ihfB* depletion with *ihfB*_P sgRNA relative to those observed with a non-targeting shuffle sgRNA (NC_159). (B, C) Mean ± SEM (n≥4) pHi values are displayed. Cultures were incubated in LB with dCas9 inducer (100ng/mL aTc) to mid-exponential phase (A_{600}~0.455-0.638) before loaded with BCECF-AM dye for cytosolic pH determination. Unpaired two-tailed t test: ***, p=0.0003; ****, p<0.0001. (D) Mean ± SEM (n≥4) pHi values are displayed for cultures first incubated in LB with dCas9 inducer (100ng/mL aTc) to early mid-exponential phase (A_{600}~0.308-0.486) then for another 1 hour with CIP 60 µg/mL prior to BCECF-AM dye loading for pHi assessment. Ordinary one-way Anova with

Šídák's multiple comparisons test: ns, adj. p=0.4989; ****, adj. p<0.0001. Untx: untreated. CIP: Ciprofloxacin. GP: *gyrAparC*. GPL: *gyrAparCadeL*.

Supplementary Figure 1: Mapping of sgRNAs shows a normal distribution of reads. Histograms of the mean reads for all sgRNAs (A) from the original pDNA library prior to introduction into *A. baumannii*; (B) after introduction in the *A. baumannii* ATCC 17978UN (WT) strain background at T1 prior to dCas9 induction (n=3); and (C) all shuffle sgRNAs in the WT strain background at T2 after dCas9 induction (50ng/mL aTc, n=3). Reads were normalized to total mapped reads and log transformed. Reads are binned by increments of 10.

Supplementary Figure 2: Lack of relationship between target location and fitness. (A-C) Statistical significance (n=10) plotted as a function of fitness differences of hypomorphs in the presence and absence of dCas9 induction (100ng/mL aTc) in the WT strain background. Gray: all sgRNAs. Black: sgRNAs overlapping start codon (A). sgRNAs that from either the 3' or 5' end of the sgRNA are 1-10nt (B) or 25-40nt (C) away from the first nt of the start codon. (B, C) Red: sgRNAs downstream the start codon. Blue: sgRNAs upstream the start codon. Dotted line: FDR or Q=5%. (D) Distribution of fitness differences (bin of 0.1) vs. fraction of perfect sgRNAs from each category falling in each fitness range. (E) Expression efficiency of four targets achieved by perfect sgRNAs that showed minimal effects on fitness are depicted alongside that of *gyrA* that shows a strong fitness defect. Efficiency is noted as the percent fold change in transcript levels observed by hypomorphs that were incubated with dCas9 inducer against those grown in parallel without inducer.

Supplementary Figure 3: Outgrowth of banks for 14-16 generations enhances fitness defects. (A, B) Statistical significance (n=5) plotted as a function of fitness scoring differences after growth for 7-8 generations compared to 14-16 generations in the presence (Black) or absence (Gray) of dCas9 induction (100ng/mL aTc) in WT (A) or GPS (B) strain backgrounds. (C-F) Statistical significance is plotted as a function of fitness changes after growth for 7-8 generations (C, E) or 14-16 generations (D, F) of all hypomorphs upon dCas9 induction. Black: perfect guides. Dark gray: statistically significant sgRNAs passing the FDR or Q=5% via multiple t-test analyses. Light gray: sgRNAs not statistically significant. Dotted red box to highlight shifts in fitness that are observed between conditions. aTc: anhydrotetracycline. WT: Wildtype. GPS: *gyrAparCadeS*.

Supplementary Figure 4: Outgrowth of banks for 14-16 generations does not substantially affect fitness of the shuffle guides. (A-D) Statistical significance (n=5) plotted as a function of fitness differences after growth for 7-8 generations (A, C) compared to 14-16 generations (B, D) of all hypomorphs upon dCas9 induction. Black: perfect guides. Dark gray: statistically significant sgRNAs passing the FDR or Q=5% via multiple t-test analyses. Light gray: sgRNAs not statistically significant. Red: shuffle sgRNAs. Dotted blue box to visualize shifts in fitness observed between conditions. WT: Wildtype. GPS: *gyrAparCadeS*.

Supplementary Figure 5: Depletion of a limited number of essential genes results in RND pump overproducer-dependent fitness defects in the absence of drug pressure. (A-C)

Statistical significance plotted as a function of the difference in fitness scores for hypomorphs in GPS (A), GPN (B), or GPL (C) vs. WT in the absence of drug after growth for 7-8 generations (n=10). Of the statistically significant sgRNAs passing the FDR or Q=5% via multiple t-test analyses (Gray), the noted targets show significant fitness score differences at least 20% from WT (limited to targets that are represented by 3 or more sgRNAs in this category, with reads of each sgRNA being at least 10 at T1, excluding ribosomal proteins). Black: sgRNAs not statistically significant. Dotted lines: selection parameters wherein substantial changes in fitness are imparted by sgRNAs. (D, E) Fitness in each strain background generated by sgRNAs of the indicated targets. Targets were identified as in A-C, however, the targets displayed fitness score differences of at least 10% from WT in all three FQR strains (D) or in two FQR strains (E). Dotted line marks neutral fitness value of 1. Untx: untreated. WT: Wildtype. GPS: *gyrAparCadeS*. GPL: *gyrAparCadeL*. GPN: *gyrAparCadeN*.

Supplementary Figure 6: Continued depletion through 14-16 generations in the absence of drug reveals a smaller set of fitness determinants tied to AdeAB overexpression than that identified after 7-8 generations. (A-B) Scatter plots of fitness resulting from indicated sgRNAs. Targets were identified after comparing fitness of hypomorphs in WT (black circles) vs. GPS (blue squares) after 7-8 generations (A, n=10) or 14-16 generations (B, n=5). The respective sgRNAs showed significant fitness score differences of at least 10% between strains, passing the FDR or Q=5% via multiple t-test analyses. Targets had to be represented by 3 or more sgRNAs, reads of each sgRNA at T1 were at least 10, and with ribosomal proteins excluded from analysis. Dotted line marks a neutral fitness value of 1. Red boxes highlight targets whose sgRNAs in

GPS yielded fitness scores that differed by at least 20% from WT. WT: Wildtype. GPS: *gyrAparCadeS*.

Supplementary Figure 7: Identification of sgRNAs that alter fitness of FQR strains relative to WT in presence of CIP. (A) Statistical significance plotted as a function of fitness score differences between hypomorphs grown in CIP and Untx conditions for 7-8 generations in the WT strain background (n=10). Gray: Statistically significant sgRNAs passing the FDR or Q=5% via multiple t-test analyses. Black circles: sgRNAs not statistically significant. 16/18 of the top targets identified as causing significantly altered fitness in the FQR strains compared to the WT strain under CIP stress are highlighted as described for Figure 3, but here in the WT strain background to depict the abated dependence on these proteins for fitness in WT. Dotted lines: selection parameters wherein substantial changes in fitness are imparted by sgRNAs. (B-C) Scatter plots exhibit the mean fitness generated by individual sgRNAs (n=10) corresponding to the 18 top FQR fitness determinants as seen in the WT (black), GPS (gray), GPN (red), or GPL (blue) strains after CIP treatment. These sgRNAs lower fitness of more than one FQR strain in the presence of CIP (B) or provide more than one FQR strain with a fitness advantage during CIP exposure (C). All unique sgRNAs are marked by circles, while the individual sgRNAs causing fitness modifications that varied significantly between FQR and WT strains (and between CIP vs Untx conditions) are labeled by empty squares. The dotted line marks the neutral fitness value of 1. CIP: ciprofloxacin. Untx: untreated. WT: wildtype. GPL: *gyrAparCadeL*. GPN: *gyrAparCadeN*. GPS: *gyrAparCadeS*.

Supplementary Figure 8: Fluctuations in hypomorph growth rates explained by varied levels of transcript depletion. (A) Mean ± SEM (n=3) growth rate differences (in min) between hypomorphs and a shuffle non-targeting control sgRNA (NC_159). Doubling time differences in untreated and CIP-treated conditions are superimposed. Unpaired t test analyses (individual variance each row) were performed on pre-selected pairs following the two-stage set-up of Benjamini, Krieger, and Yekutieli with a false discovery rate of 5% (30). Target depletions yielding significant differences in doubling times between GPL and WT during CIP exposure are shown: *, $p<0.05$; **, $p<0.02$; ***, $p<0.01$; ****, $p<0.001$. (B) Mean fold change ($2^{\Delta\Delta CT}$) ± SEM (n=3) in transcript levels for each target as compared to a non-targeting shuffle sgRNA control (NC_159) in the WT (light gray) and GPL (dark gray) strain backgrounds. Arrows (A, B) point to the unique sgRNAs yielding unanticipated fitness results. (C) Mean fold change ($2^{-\Delta\Delta CT}$) ± SEM (n=3) in transcript levels of *atpF* in GPL during depletion using sgRNA AtpF_20 compared to those observed using a non-targeting shuffle sgRNA (NC_1). The value inside the bar: mean transcript level ($2^{-\Delta\Delta CT}$) relative to the shuffle control; value outside the bar: knockdown efficiency ($2^{\Delta\Delta CT}$) compared to shuffle control. (B, C) Values are negative to display lowered transcript levels resulting from the targeted depletions. CIP: ciprofloxacin (50 µg/mL for GPL and 0.09 µg/mL for WT). Untx: untreated. WT: wildtype. GPL: *gyrAparCadeL*.

Supplementary Figure 9: Variability during LpxC and LptC depletion. (A) Mean ± SEM (n=9) growth rate differences (in min) between hypomorphs and a shuffle non-targeting control sgRNA (NC_159). Unpaired t test analyses (individual variance each row) were performed on pre-selected pairs following the two-stage set-up of Benjamini, Krieger, and Yekutieli with a false discovery rate of 5% (30). Target depletions yielding significant differences in doubling

times between GPL and WT during CIP exposure are shown: ****, p=0.000007. (B) Mean fold change ($2^{\Delta\Delta CT}$) ± SEM (n=9) in transcript levels for each target as compared to a non-targeting shuffle sgRNA control (NC_159) in the WT (black border) and GPL (gray border) strain backgrounds. Transcript levels were evaluated via qRT-PCR in samples harvested from cultures grown in the absence of drug. Values are negative to portray lowered transcript levels resulting from the targeted depletions, and the mean values are noted above the x-axis. (A-B) Color of each data point represents a biological replicate to better relate repression and growth rate results. CIP: ciprofloxacin (50 µg/mL for GPL and 0.09 µg/mL for WT). Untx: untreated. WT: wildtype. GPL: *gyrAparCadeL*.

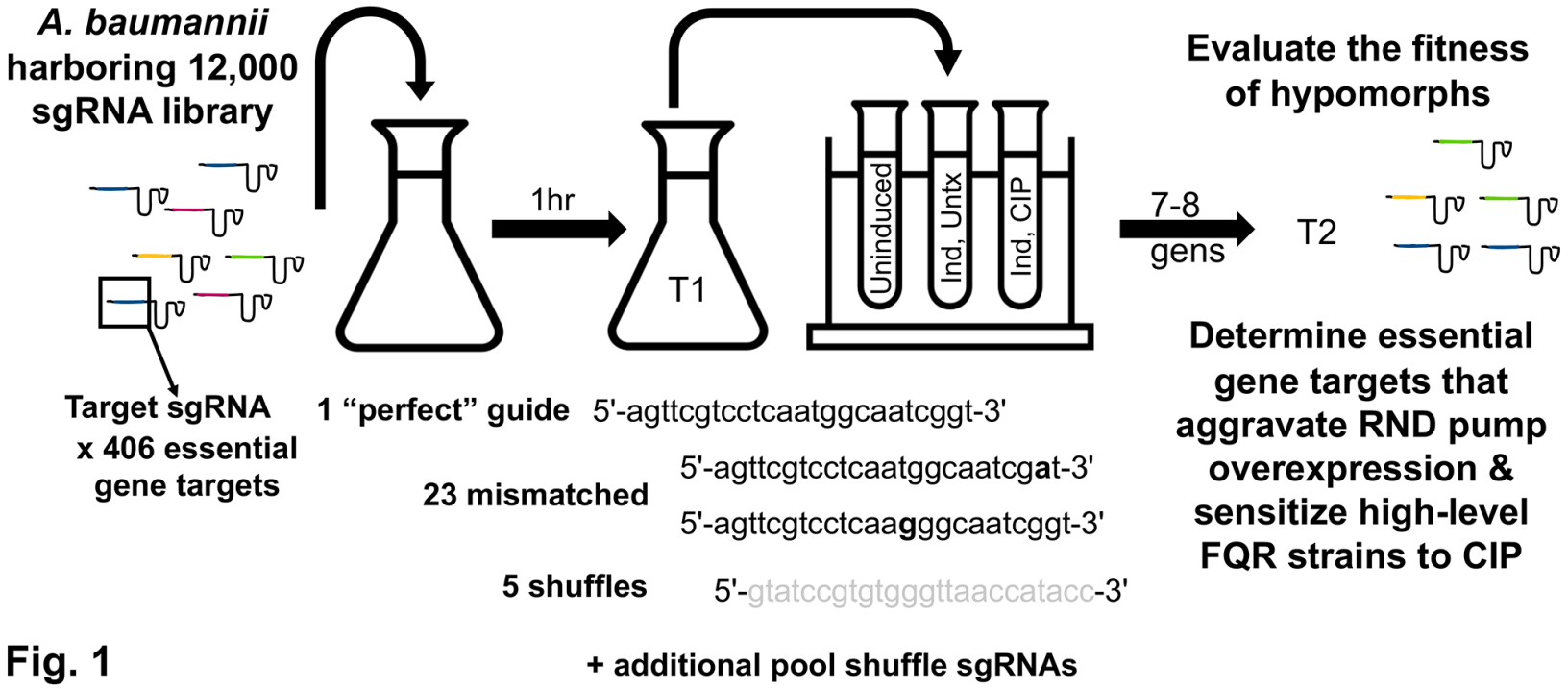
A. baumannii harboring 12,000 sgRNA library
Target sgRNA x 406 essential gene targets
1hr
T1
Uninduced
Ind, Untx
Ind, CIP
7-8 gens
T2
Evaluate the fitness of hypomorphs
Determine essential gene targets that aggravate RND pump overexpression & sensitize high-level FQR strains to CIP
1 "perfect" guide 5'-agttcgtcctcaatggcaatcggt-3'
23 mismatched
5'-agttcgtcctcaatggcaatcgat-3'
5'-agttcgtcctcaagggcaatcggt-3'
5 shuffles 5'-gtatccgtgtgggttaaccatacc-3'
+ additional pool shuffle sgRNAs

Fig. 1

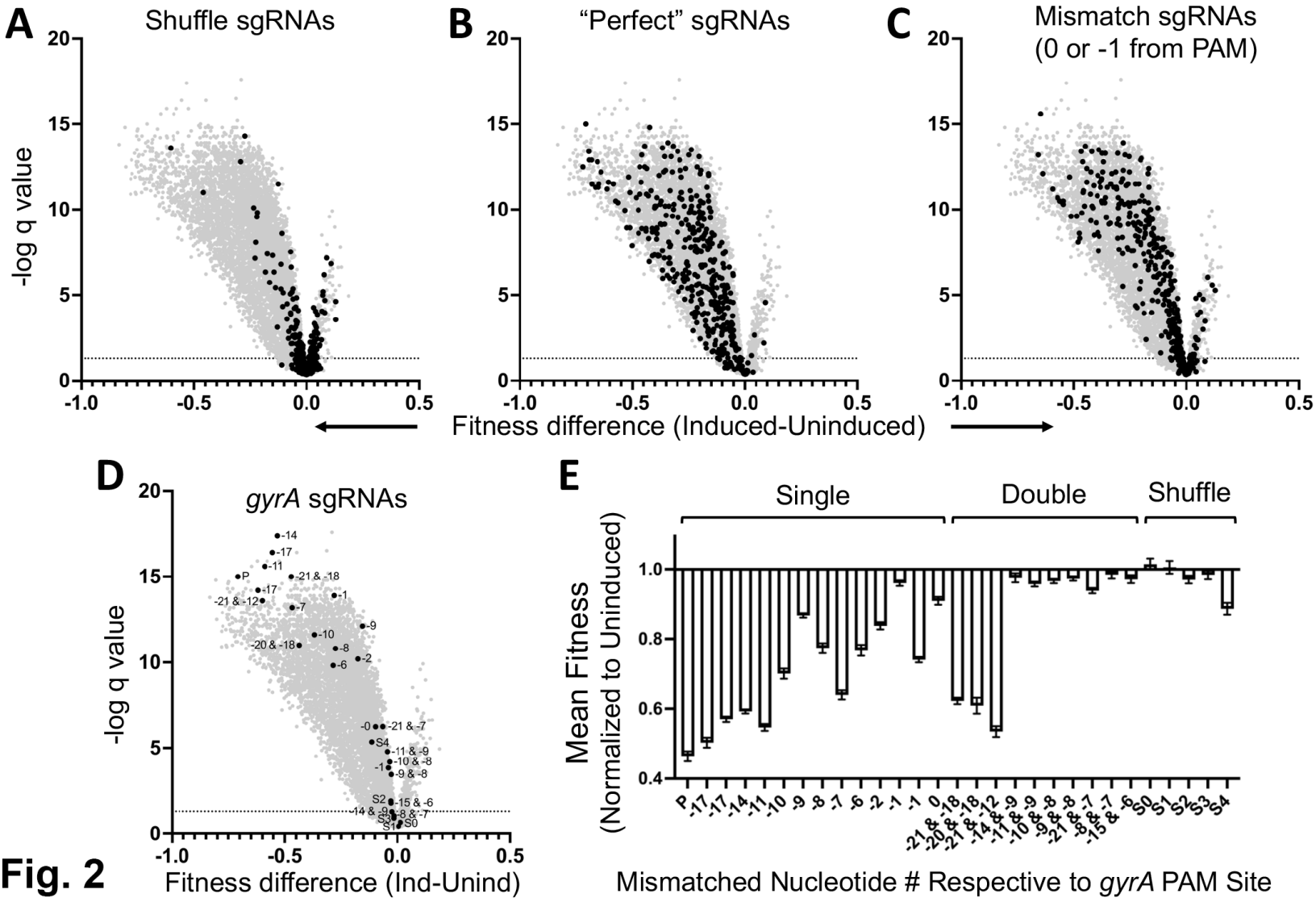
A
Shuffle sgRNAs
B
"Perfect" sgRNAs
C
Mismatch sgRNAs
(0 or -1 from PAM)
-log q value
Fitness difference (Induced-Uninduced)
D
gyrA sgRNAs
-log q value
Fitness difference (Ind-Unind)
E
Single
Double
Shuffle
Mean Fitness
(Normalized to Uninduced)
Mismatched Nucleotide # Respective to gyrA PAM Site

Fig. 2

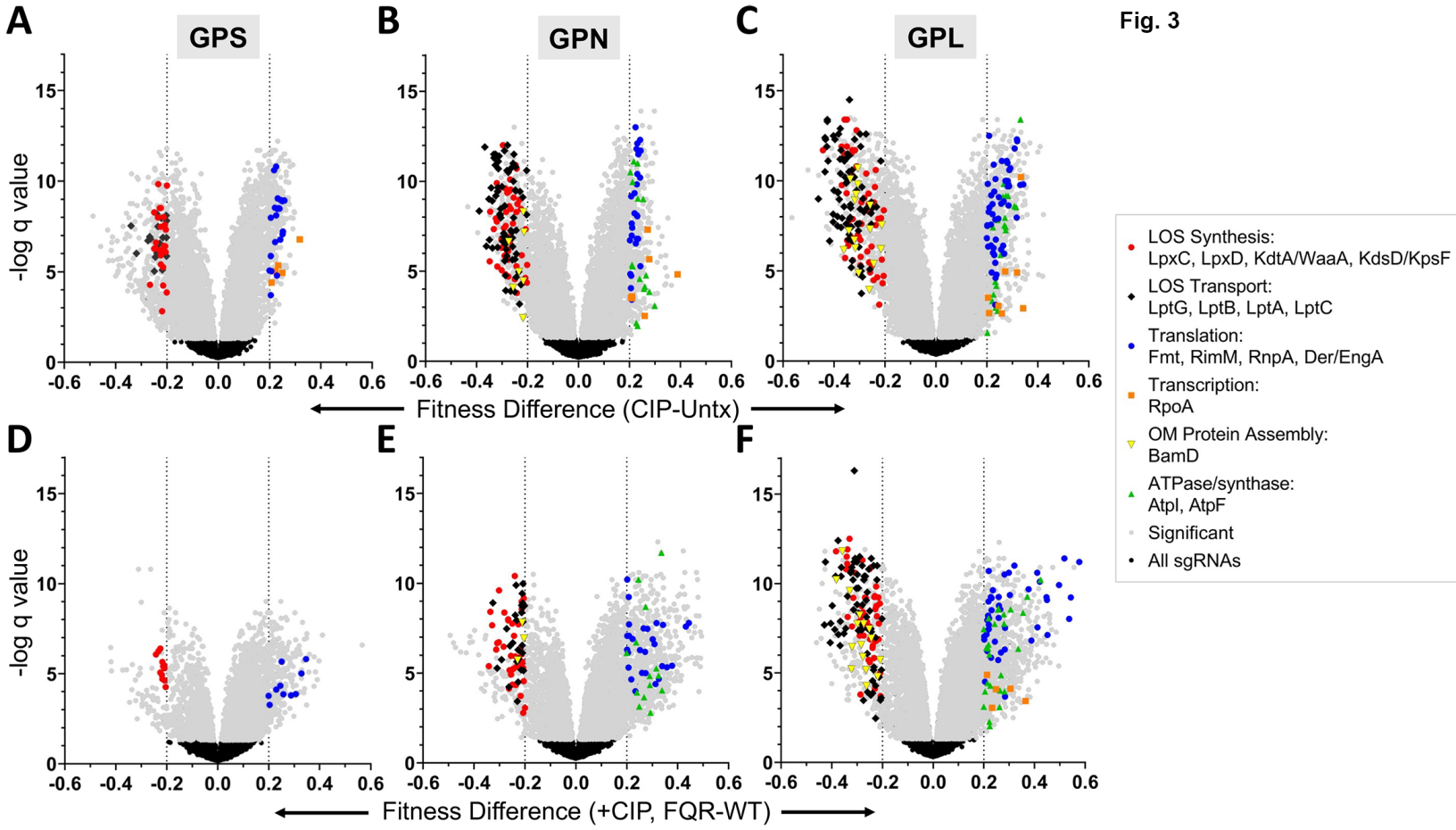
A
GPS
B
GPN
C
GPL
D
E
F
-log q value
Fitness Difference (CIP-Untx)
Fitness Difference (+CIP, FQR-WT)
LOS Synthesis:
LpxC, LpxD, KdtA/WaaA, KdsD/KpsF
LOS Transport:
LptG, LptB, LptA, LptC
Translation:
Fmt, RimM, RnpA, Der/EngA
Transcription:
RpoA
OM Protein Assembly:
BamD
ATPase/synthase:
AtpI, AtpF
Significant
All sgRNAs

Fig. 3

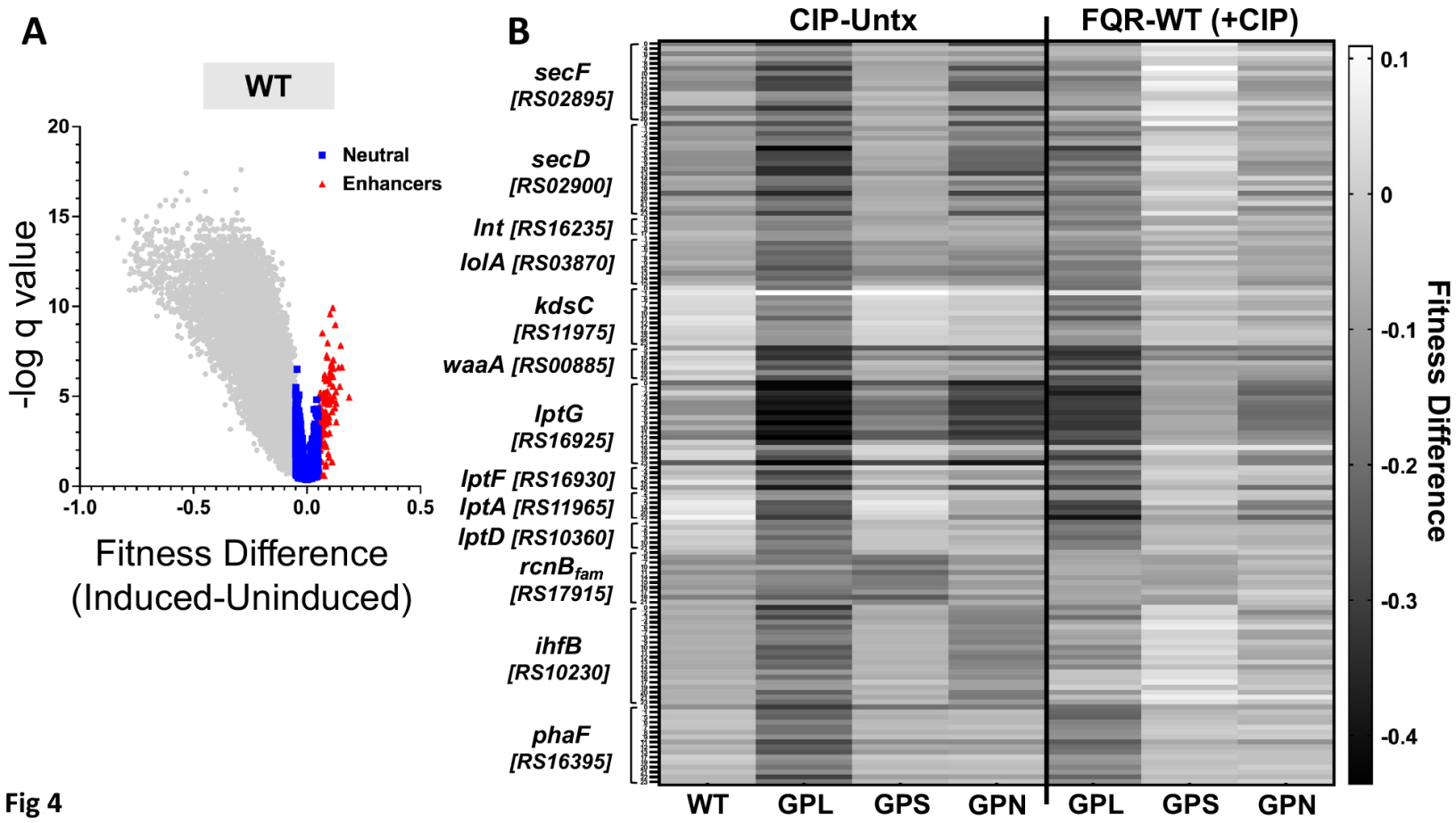
A
WT
Neutral
Enhancers
-log q value
Fitness Difference
(Induced-Uninduced)
B
CIP-Untx
FQR-WT (+CIP)
secF [RS02895]
secD [RS02900]
lnt [RS16235]
lolA [RS03870]
kdsC [RS11975]
waaA [RS00885]
lptG [RS16925]
lptF [RS16930]
lptA [RS11965]
lptD [RS10360]
rcnB fam [RS17915]
ihfB [RS10230]
phaF [RS16395]
WT
GPL
GPS
GPN
GPL
GPS
GPN
Fitness Difference

Fig 4

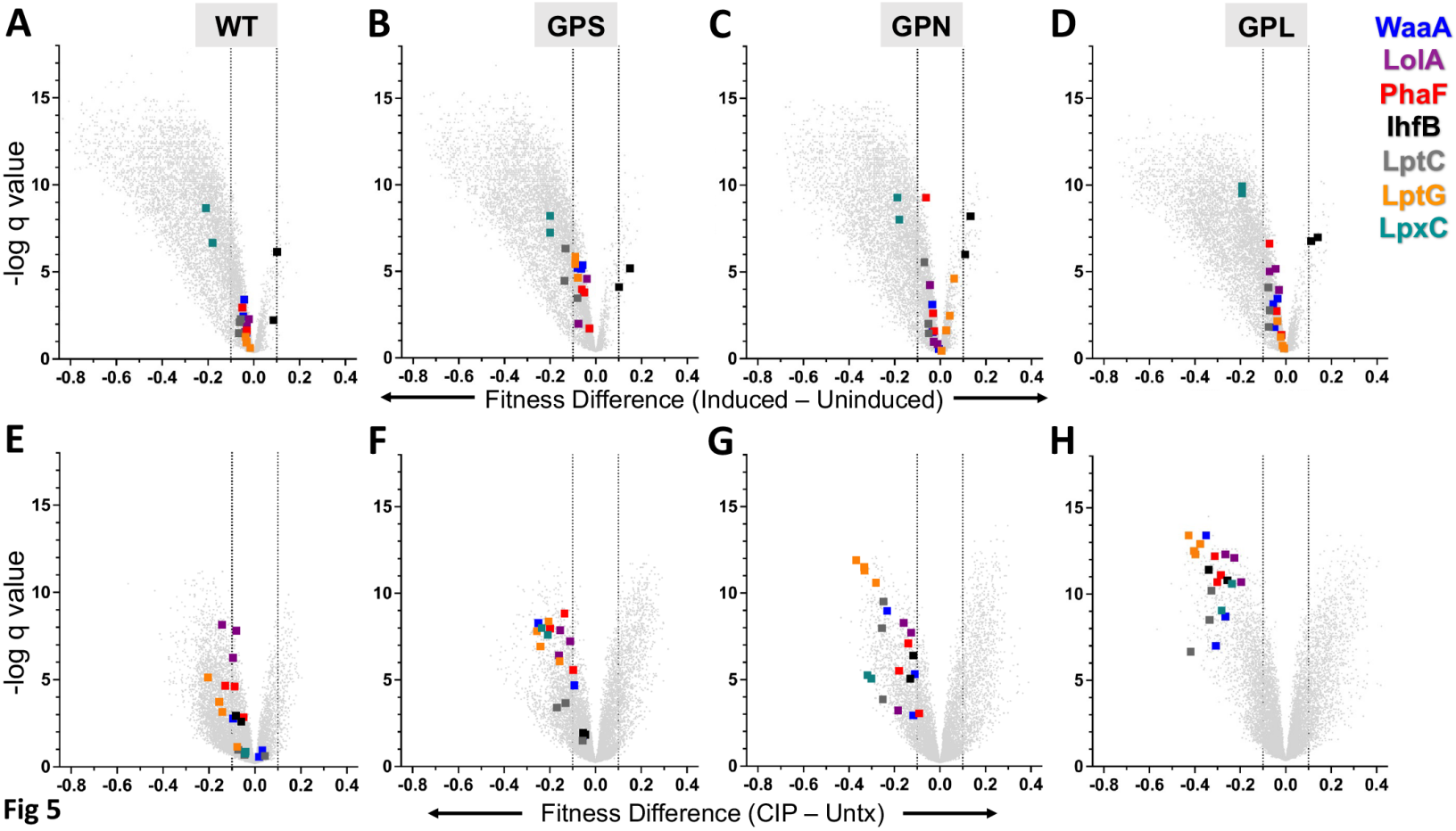
A
WT
B
GPS
C
GPN
D
GPL
WaaA
LolA
PhaF
IhfB
LptC
LptG
LpxC
-log q value
Fitness Difference (Induced – Uninduced)
E
F
G
H
-log q value
Fitness Difference (CIP – Untx)

Fig 5

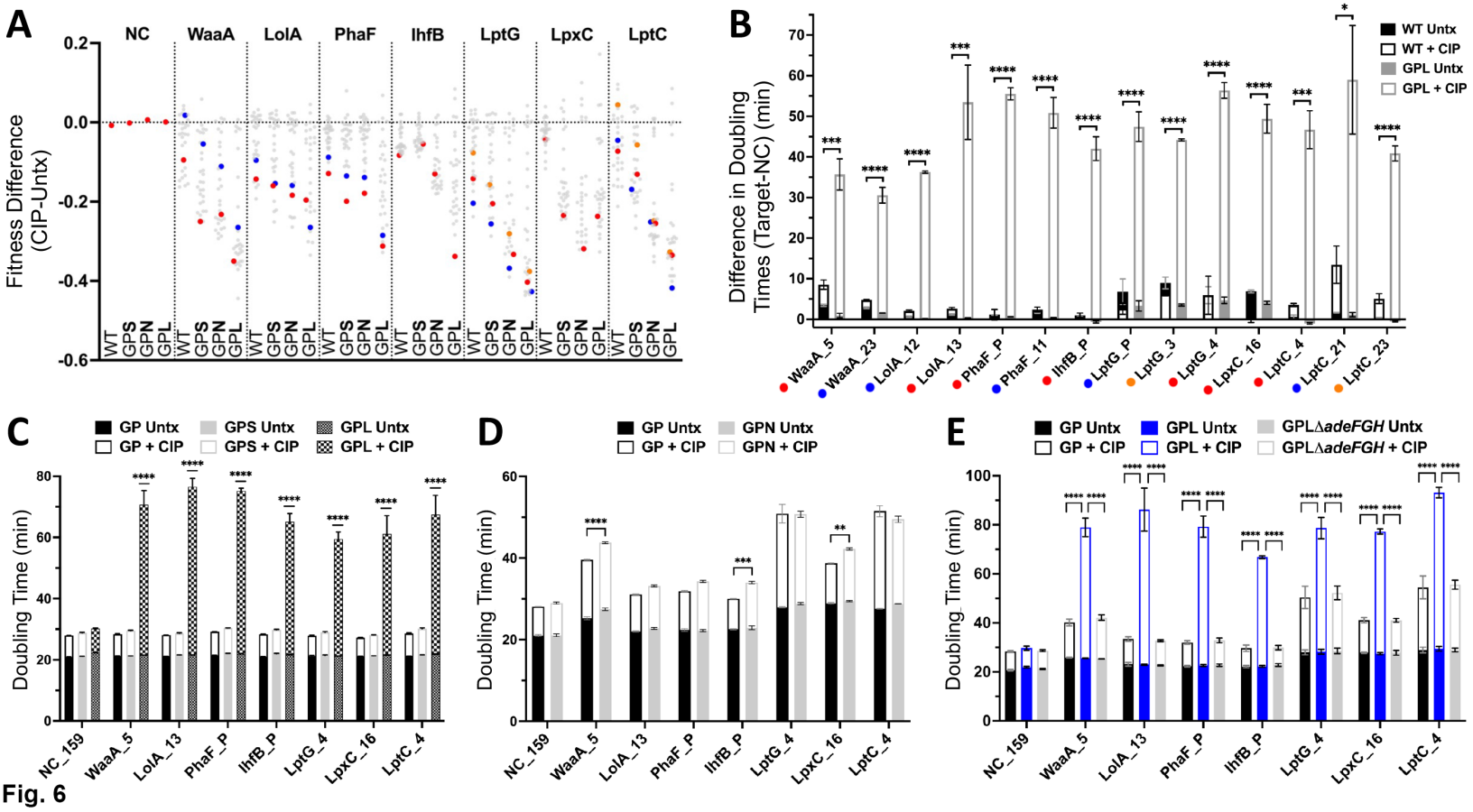
A
NC
WaaA
LolA
PhaF
IhfB
LptG
LpxC
LptC
Fitness Difference (CIP-Untx)
WT
GPS
GPN
GPL
B
Difference in Doubling Times (Target-NC) (min)
WT Untx
WT + CIP
GPL Untx
GPL + CIP
WaaA_5
WaaA_23
LolA_12
LolA_13
PhaF_P
PhaF_11
IhfB_P
LptG_P
LptG_3
LptG_4
LpxC_16
LptC_4
LptC_21
LptC_23
C
GP Untx
GP + CIP
GPS Untx
GPS + CIP
GPL Untx
GPL + CIP
Doubling Time (min)
NC_159
WaaA_5
LolA_13
PhaF_P
IhfB_P
LptG_4
LpxC_16
LptC_4
D
GP Untx
GP + CIP
GPN Untx
GPN + CIP
Doubling Time (min)
E
GP Untx
GP + CIP
GPL Untx
GPL + CIP
GPLΔadeFGH Untx
GPLΔadeFGH + CIP
Doubling Time (min)

Fig. 6

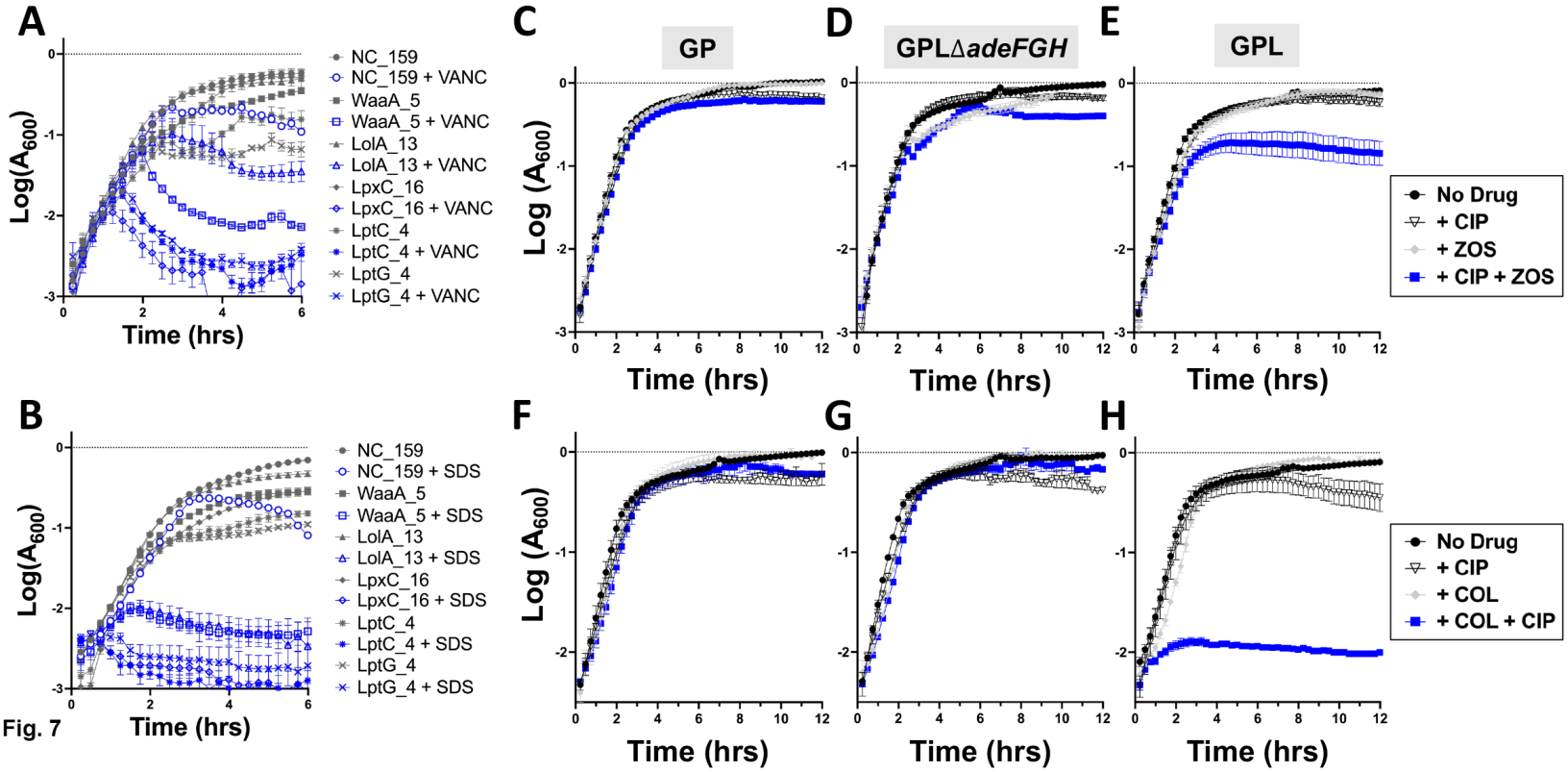
A
Log(A600)
Time (hrs)
NC_159
NC_159 + VANC
WaaA_5
WaaA_5 + VANC
LolA_13
LolA_13 + VANC
LpxC_16
LpxC_16 + VANC
LptC_4
LptC_4 + VANC
LptG_4
LptG_4 + VANC
B
Log(A600)
Time (hrs)
NC_159
NC_159 + SDS
WaaA_5
WaaA_5 + SDS
LolA_13
LolA_13 + SDS
LpxC_16
LpxC_16 + SDS
LptC_4
LptC_4 + SDS
LptG_4
LptG_4 + SDS
C
GP
D
GPLΔadeFGH
E
GPL
Log (A600)
Time (hrs)
No Drug
+ CIP
+ ZOS
+ CIP + ZOS
F
G
H
Log (A600)
Time (hrs)
No Drug
+ CIP
+ COL
+ COL + CIP

Fig. 7

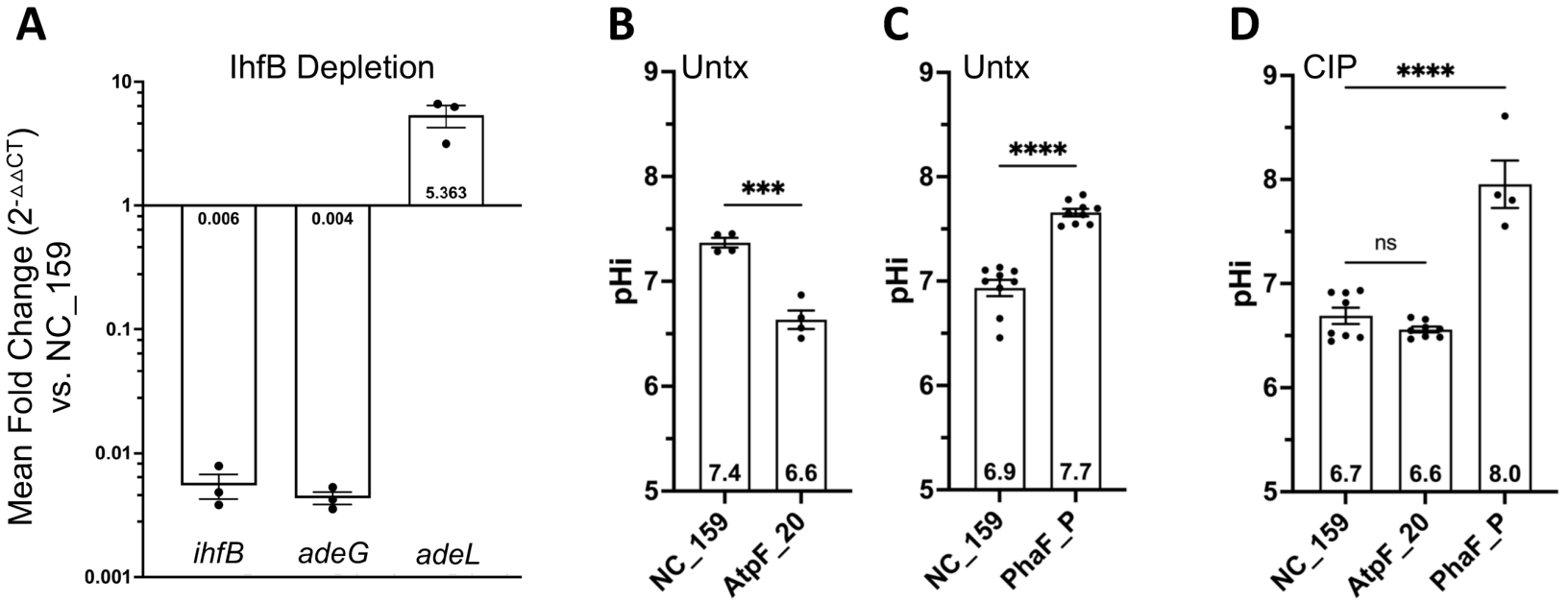
A
IhfB Depletion
Mean Fold Change ($2^{-\Delta\Delta CT}$) vs. NC_159
10
1
0.1
0.01
0.001
0.006
0.004
5.363
ihfB
adeG
adeL
B
Untx
pHi
9
8
7
6
5
***
7.4
6.6
NC_159
AtpF_20
C
Untx
pHi
****
6.9
7.7
NC_159
PhaF_P
D
CIP
pHi
****
ns
6.7
6.6
8.0
NC_159
AtpF_20
PhaF_P

Fig 8